COMILLAS
UNIVERSIDAD PONTIFICIA
ICAI

GRADO EN INGENIERÍA EN TECNOLOGÍAS INDUSTRIALES

TRABAJO FIN DE GRADO

Analysis of avian tail aerodynamics for improved flying efficiency

Autor: Andrés Miguélez Tato

Director: Enrico Ajanic

Madrid

July 2020

I, hereby, declare that I am the only author of the project report with title:

Analysis of avian tail aerodynamics for improved flying efficiency

which has been submitted to ICAI School of Engineering of Comillas Pontifical University in the academic year 2020/21. This project is original, has not been submitted before for any other purpose and has not been copied from any other source either fully or partially. All information sources used have been rightly acknowledged.

Signed: Andrés Miguélez Date: 20/07/2021

I authorize the submission of this project

PROJECT SUPERVISOR

Signed: Enrico Ajanic Date: 20/07/2021

AUTHORIZATION FOR DIGITALIZATION, STORAGE AND DISSEMINATION IN THE NETWORK OF END-OF-DEGREE PROJECTS, MASTER PROJECTS, DISSERTATIONS OR BACHILLERATO REPORTS

1. Declaration of authorship and accreditation thereof.

The author Mr./Ms.___Andrés Miguélez Tato_____
HEREBY DECLARES that he/she owns the intellectual property rights regarding the piece of work:
_____ Analysis of avian tail aerodynamics for improved flying efficiency_____
that this is an original piece of work, and that he/she holds the status of author, in the sense granted by the Intellectual Property Law.

2. Subject matter and purpose of this assignment.

With the aim of disseminating the aforementioned piece of work as widely as possible using the University's Institutional Repository the author hereby **GRANTS** Comillas Pontifical University, on a royalty-free and non-exclusive basis, for the maximum legal term and with universal scope, the digitization, archiving, reproduction, distribution and public communication rights, including the right to make it electronically available, as described in the Intellectual Property Law. Transformation rights are assigned solely for the purposes described in a) of the following section.

3. Transfer and access terms

Without prejudice to the ownership of the work, which remains with its author, the transfer of rights covered by this license enables:

a) Transform it in order to adapt it to any technology suitable for sharing it online, as well as including metadata to register the piece of work and include "watermarks" or any other security or protection system.

b) Reproduce it in any digital medium in order to be included on an electronic database, including
the right to reproduce and store the work on servers for the purposes of guaranteeing its security,
maintaining it and preserving its format.

c) Communicate it, by default, by means of an institutional open archive, which has open and cost-free online access.

d) Any other way of access (restricted, embargoed, closed) shall be explicitly requested and requires that good cause be demonstrated.

e) Assign these pieces of work a Creative Commons license by default.

f) Assign these pieces of work a HANDLE (persistent URL). by default.

4. Copyright.

The author, as the owner of a piece of work, has the right to:

a) Have his/her name clearly identified by the University as the author

b) Communicate and publish the work in the version assigned and in other subsequent versions using any medium.

c) Request that the work be withdrawn from the repository for just cause.

d) Receive reliable communication of any claims third parties may make in relation to the work and, in particular, any claims relating to its intellectual property rights.

5. Duties of the author.

The author agrees to:

a) Guarantee that the commitment undertaken by means of this official document does not infringe any third party rights, regardless of whether they relate to industrial or intellectual property or any other type.

b) Guarantee that the content of the work does not infringe any third party honor, privacy or image rights.

c) Take responsibility for all claims and liability, including compensation for any damages, which may be brought against the University by third parties who believe that their rights and interests have been infringed by the assignment.

d) Take responsibility in the event that the institutions are found guilty of a rights infringement regarding the work subject to assignment.

6. Institutional Repository purposes and functioning.

The work shall be made available to the users so that they may use it in a fair and respectful way with regards to the copyright, according to the allowances given in the relevant legislation, and for study or research purposes, or any other legal use. With this aim in mind, the University undertakes the following duties and reserves the following powers:

a) The University shall inform the archive users of the permitted uses; however, it shall not guarantee or take any responsibility for any other subsequent ways the work may be used by users, which are non-compliant with the legislation in force. Any subsequent use, beyond private copying, shall require the source to be cited and authorship to be recognized, as well as the guarantee not to use it to gain commercial profit or carry out any derivative works.

b) The University shall not review the content of the works, which shall at all times fall under the exclusive responsibility of the author and it shall not be obligated to take part in lawsuits on behalf of the author in the event of any infringement of intellectual property rights deriving from storing and archiving the works. The author hereby waives any claim against the University due to any way the users may use the works that is not in keeping with the legislation in force.

c) The University shall adopt the necessary measures to safeguard the work in the future.

d) The University reserves the right to withdraw the work, after notifying the author, in sufficiently justified cases, or in the event of third party claims.

Madrid, on ……July 20th..……. , ……2021….

HEREBY ACCEPTS

Signed……  ……

Reasons for requesting the restricted, closed or embargoed access to the work in the Institution's

COMILLAS
UNIVERSIDAD PONTIFICIA
ICAI

GRADO EN INGENIERÍA EN TECNOLOGÍAS INDUSTRIALES

TRABAJO FIN DE GRADO

Analysis of avian tail aerodynamics for improved flying efficiency

Autor: Andrés Miguélez Tato

Director: Enrico Ajanic

Madrid

July 2020

ANÁLISIS AERODINÁMICO DE LA COLA AVIAR PARA UNA MEJOR EFICIENCIA DE VUELO

Autor: Miguélez Tato, Andrés.
Director: Ajanic, Enrico.
Entidad Colaboradora: Laboratory of Intelligent Systems – EPFL

RESUMEN DEL PROYECTO

Se fabricaron tres colas inspiradas en aves (circular, triangular y ahorquillada) y se montaron sobre un fuselaje, previo paso a ponerlas a prueba en un túnel de viento. Los resultados muestran que la cola con perfil triangular es la más eficiente, según indica el cociente entre sustentación y arrastre. Otros resultados del estudio son que el fuselaje afecta el flujo de aire en la cola y permite al conjunto completo generar más sustentación, pero también más arrastre.

Palabras clave: Cola aviar, aerodinámica, sustentación, arrastre.

1. Introducción

En el mercado de drones actual no existe un dispositivo que sea a la vez ágil y rápido, capaz de volar por los árboles de un bosque o a través de los semáforos, edificios y monumentos de una ciudad. En una sociedad que demanda cada vez más drones para llevar a cabo tareas de lo más diverso como vigilancia, reparto o comunicaciones, parece más que justificado invertir tiempo y dinero en mejorar sus capacidades de vuelo.

Al observar la naturaleza se puede apreciar que las aves consiguen exactamente los que los drones no: éstas pueden volar con velocidad (en caída hacia una presa, por ejemplo) y también con agilidad (describiendo curvas cerradas cerca de árboles), por lo que es una buena idea basarse en ellas para así mejorar los drones artificiales. Uno de los elementos que los pájaros utilizan para volar con tanta destreza es su cola, que les proporciona los momentos necesarios para la guiñada y el cabeceo [1] pero también reduce el arrastre del animal [2]. No obstante, los estudios acerca de la cola aviar no coinciden en los parámetros que determinan el rendimiento de esta superficie. Por ejemplo, algunos autores afirman que la envergadura de la cola fija la sustentación que genera y su área determina el arrastre [3], mientras otros sostienen que cuanto más se recorta la cola, mayor es el arrastre.

2. Definición del proyecto

El objetivo principal de este proyecto es determinar cómo afecta la forma de la cola a las características aerodinámicas de drones. Sin embargo, estudios previos aplican enfoques muy diferentes a este problema (algunos son puramente teóricos mientras que otros son más prácticos), además de no coincidir en los resultados. Por lo tanto, este proyecto se llevará a cabo ensayando las colas en un túnel de viento.

Se van a fabricar distintas colas inspiradas en pájaros, así como un fuselaje que actuará como el cuerpo del ave. Estas piezas se van a ensayar en un túnel de viento, a distintas velocidades y ángulos de ataque (mismo número de Reynolds en las colas) y se medirán las fuerzas generadas.

3. Descripción del sistema

El fuselaje y las colas conforman el pájaro ficticio (dron) objeto de estudio. La disposición de los elementos se muestra en la Ilustración 1. Una vara de metal sujeta firmemente el conjunto que se va a ensayar y lo conecta con el brazo robótico, que cambia el ángulo de ataque entre 0 y 45 grados. Una serie de ventiladores proporcionan el viento, en velocidades de 0 a 10 m/s, simulando así el vuelo del dron. Se va a ensayar el fuselaje con cada una de las colas, pero también las colas por separado (ver Ilustración 1).

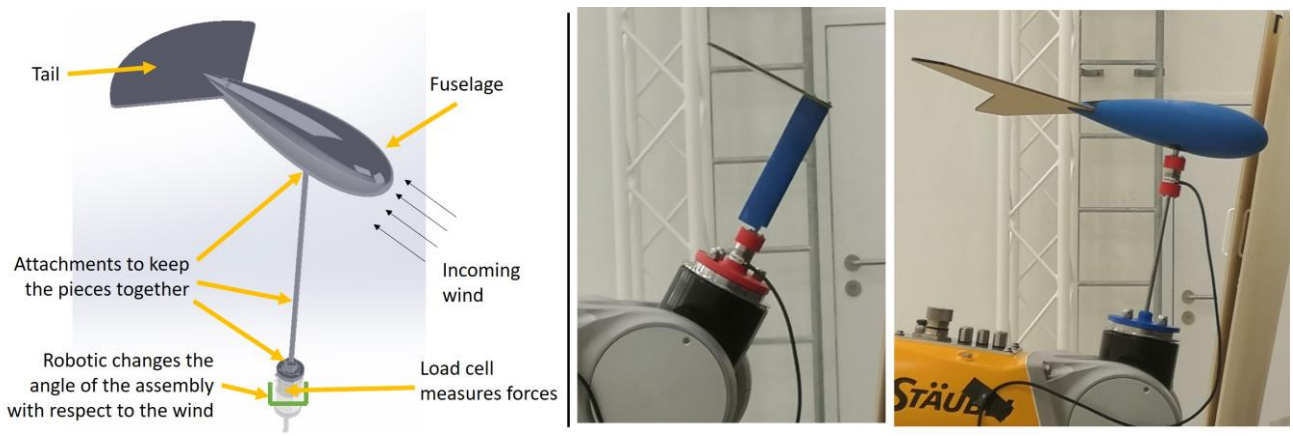

Ilustración 1. Disposición teórica y experimental.

Durante todo este proceso una célula de carga medirá las fuerzas ejercidas por el viento, que a su vez se usarán para calcular la sustentación y el arrastre que provoca cada cola.

4. Resultados

Las 3 colas entran en pérdida a unos 20-25º, generado un coeficiente de sustentación similar dentro de una ventana de 0,1. El coeficiente de sustentación más elevado se sitúa sobre 0,7, conseguido por la cola ahorquillada justo antes de entrar en pérdida a la mayor velocidad (10 m/s). El coeficiente de arrastre es independiente de la forma de la cola y de la velocidad de vuelo, y solo varía con el ángulo de ataque. En cuanto a la relación sustentación-arrastre, la Ilustración 2 muestra que la cola triangular ofrece mayores valores para ángulos de ataque bajos, sin embargo, esta diferencia va desapareciendo conforme aumenta el ángulo de ataque.

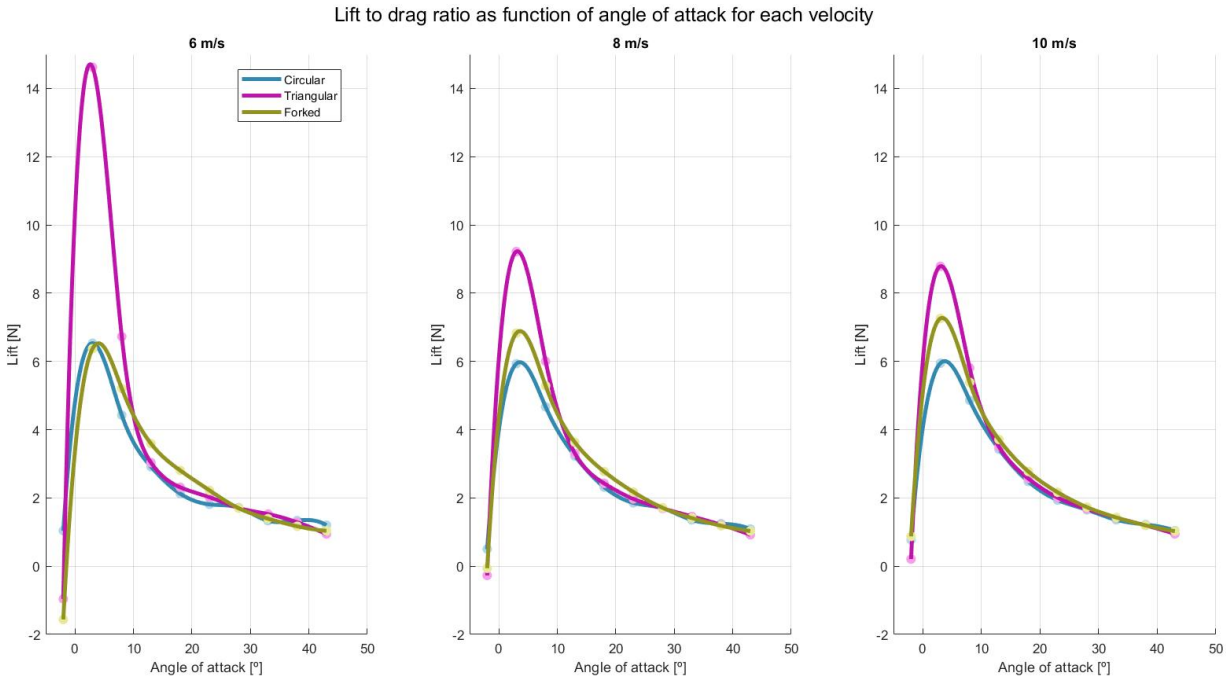

Ilustración 2. Cociente sustentación-arrastre de las 3 colas.

Además, la Ilustración 3 indica que las fuerzas (sustentación y arrastre) generadas por la cola son similares cuando esta va montada en el fuselaje y cuando no. No obstante, si el ángulo de ataque sobrepasa 20º (ángulo de pérdida de la cola), la cola produce fuerzas significativamente mayores cuando está montada en el fuselaje.

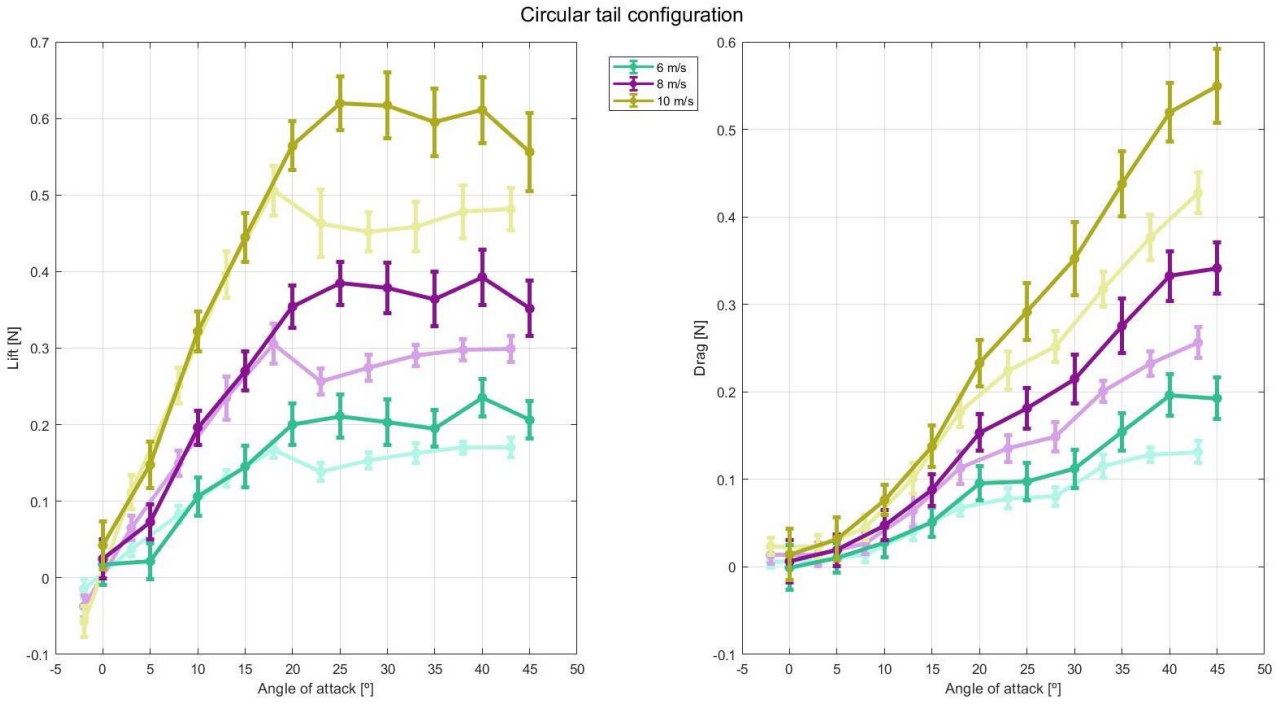

Ilustración 3. Sustentación y arrastre creados por la cola en las dos configuraciones de la cola circular. Los colores fuertes corresponden a la cola montada en el fuselaje, mientras que los colores tenues corresponden a la cola sin fuselaje. Las barras indican la desviación estándar.

5. Conclusiones

Cuando vuelan con el mismo número de Reynolds, la cola que mejor rinde, según el cociente sustentación-arrastre, es la triangular, lo cual sería la solución óptima si el objetivo del dron fuera cubrir largas distancias. Sin embargo, si lo que interesa es solamente la sustentación, la cola ahorquillada es la mejor, posiblemente debido a su mayor relación de aspecto. Además, el cuerpo del ave (o dron) altera el flujo de aire alrededor de la cola. El fuselaje permite que el flujo se desprenda a mayores ángulos de ataque, retrasando así la entrada en pérdida y produciendo fuerzas mayores.

6. Referencias

[1] Taylor, G. K. & Thomas, A. L. R. Animal flight dynamics II. Longitudinal stability in flapping flight. *Journal of Theoretical Biology* 351-370 (2002).

[2] Maybury, W. J. & Rayner, J. The avian tail reduces body parasite drag by controlling flow separation and vortex shedding. *The Royal Society* 1405-1410 (2001).

[3] Thomas, A. L. R. On the aerodynamics of birds' tails. *Philosophical transactions: Biological Sciences* **340**, 361-380 (1993).

ANALYSIS OF AVIAN TAIL AERODYNAMICS FOR IMPROVED FLYING EFFICIENCY

Author: Miguélez Tato, Andrés.
Supervisor: Ajanic, Enrico.
Collaborating Entity: Laboratory of Intelligent Systems – EPFL

ABSTRACT

Three different avian inspired tails (circular, triangular and forked) were manufactured and mounted on a fuselage to test their aerodynamics in a wind tunnel. The results show that the triangular tail performs the best, as measured by its lift to drag ratio. Other findings show that the fuselage alters the airflow around the tails and allows the whole assembly to generate higher lift, but also produces a higher drag.

Keywords: Avian tail, aerodynamics, lift, drag.

1. Introduction

The current drone market lacks a device that can be both agile and fast, capable of flying through the trees of a forest or the buildings, traffic lights and monuments of cities. In a society that demands ever more drones to carry out a wide range of tasks like delivery, surveillance or communication, it seems appropriate to spend time and effort in improving their flying capabilities.

Looking at nature, one can see that birds achieve exactly what drones cannot: they can fly fast (when diving for prey, for example) and agile (when bending sharp turns around trees), so it is a good idea to take inspiration from them in order to improve man-made drones. One of the things that enables birds to fly so swiftly is their tail, providing them the necessary torques for pitching and yawing [1], but also reducing the drag [2]. However, research on the avian tail does not conclude which parameters determine the performance of this airfoil, as authors tend to disagree on this. For instance, some claim that it is the span of the tail what determines the lift it generates, and the area determines the drag [3], where others state that the more the tail is trimmed, the bigger the drag [2].

2. Project definition.

The main goal of this project is to find out how different shapes of avian inspired tails affect the aerodynamics of drones. However, previous studies found in literature apply very different approaches to this (some purely theoretical while others more practical) and, on top of that, do not agree on the results. Therefore, the way to carry out this project is to test the tails in a wind tunnel.

Several tails will be manufactured, as well as a fuselage to mount them on. These pieces will then be tested in a wind tunnel, at different wind speeds and angles of attack (same Reynolds number across tails), and the forces generated will be measured.

3. Description of the system

The fuselage and the tails will create our dummy bird (drone), which is the main object of study. The setup is shown in Illustration 1. A metal rod will hold in place the assembly to be tested, as well as connect it to a robotic arm that changes the angle of attack from

0 to 45 degrees. An array of fans provides the wind, ranging from 0 to 10 m/s, simulating the flight of the drone. We will test the fuselage with each of the three tails, but also each of the tails on its own, as seen in Illustration 1.

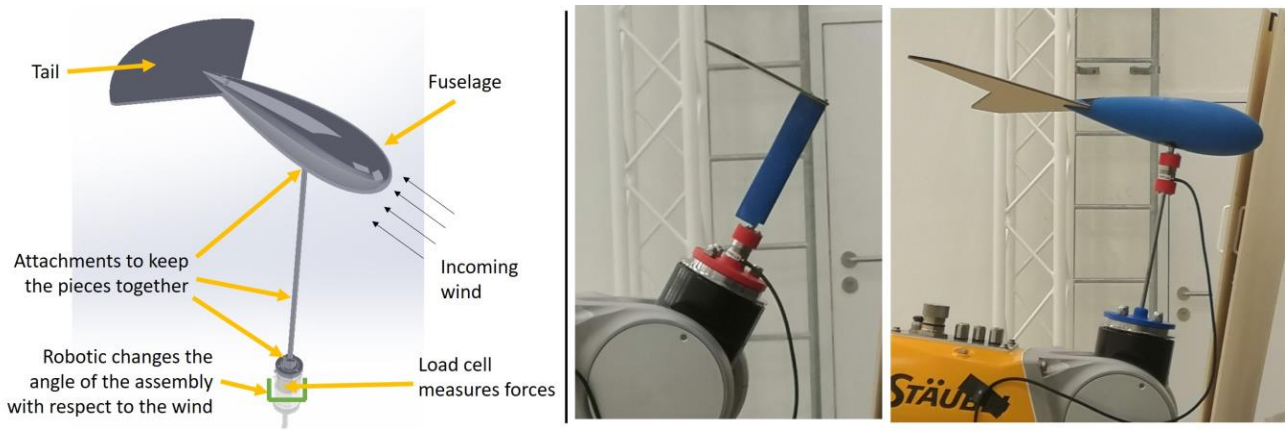

Illustration 1. Conceived and experimental setups.

Throughout this process we will measure the forces generated by the wind via a load cell, which will be used in turn to calculate the lift and the drag each tail generates.

4. Results

All 3 tails stall at about 20-25º, generating a similar lift coefficient within a 0.1 window. The highest lift coefficient is around 0.7, achieved by the forked tail just before stalling, at the maximum flying speed (10 m/s). The drag coefficient is independent of the shape of the tail and the speed at which it flies, varying only as the angle of attack does. In terms of lift to drag ratio, Illustration 2 below shows that the triangular tail offers the highest values at low angles of attack, however this difference disappears as the angle of attack increases.

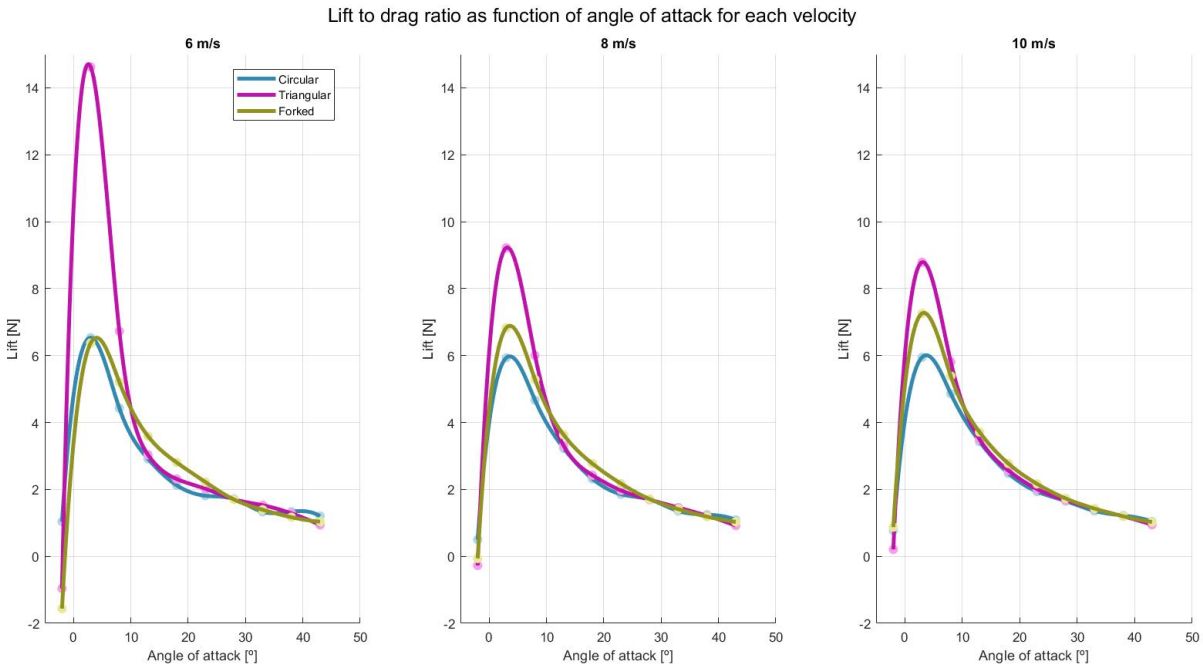

Illustration 2. Lift to drag ratio of the 3 tails.

Furthermore, Illustration 3 indicates that the forces (lift and drag) generated by the tail are similar when the tail is attached to the fuselage and when it is not. However, when the angle of attack surpasses 20º (stalling angle of the tail), the tail produces considerably greater forces if attached to the fuselage.

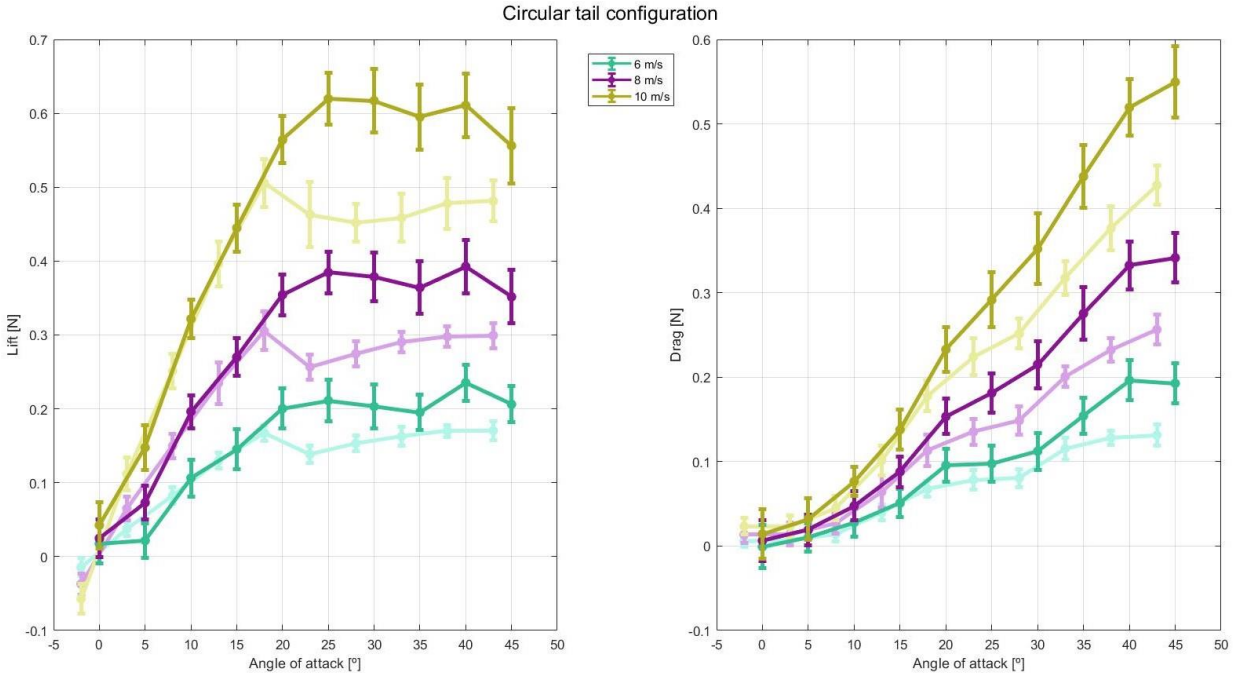

Illustration 3. Aerodynamics of the tail for the two assemblies that encompass the circular tail. Strong colours correspond to the fuselage-tail assembly, while faint ones correspond to the tail by itself. Bars show standard deviation.

5. Conclusions

When flying at matching Reynolds number, the best performant tail, as measured by the lift to drag ratio, is the triangular one, which would be the preferred solution if the aim of the drone were to cover long distances. However, if it is pure lift what we are interested in, then the forked tail is best, probably due to its higher aspect ratio. Moreover, the body of the bird (or drone) modifies the airflow around the tail. The fuselage enables the flow of air to hold on to the tail at higher angles of attack, delaying the stall and producing higher forces.

6. References

[1] Taylor, G. K. & Thomas, A. L. R. Animal flight dynamics II. Longitudinal stability in flapping flight. *Journal of Theoretical Biology* 351-370 (2002).

[2] Maybury, W. J. & Rayner, J. The avian tail reduces body parasite drag by controlling flow separation and vortex shedding. *The Royal Society* 1405-1410 (2001).

[3] Thomas, A. L. R. On the aerodynamics of birds' tails. *Philosophical transactions: Biological Sciences* **340**, 361-380 (1993).

Document index

Index of figures

Index of tables

Chapter 1. INTRODUCTION

Birds can achieve fantastic flying performances where drones as we know them today cannot. The necessity to fly over cities or forests for surveillance, reconnaissance or rescue missions asks for more advanced drones, capable of different flying styles, in an avian manner. While birds can be both agile and fast, bending sharp turns, gliding or diving for prey, the drones available on the market have to choose for either speed (classic plane-like drone) or agility (quadrotor).

Figure 1. Different types of drones: quadrotor (left) and fixed wing aircraft (right).

When comparing a plane with a bird, one cannot help to notice the difference between their tails. While most planes employ some sort of T-shaped tail that provides the necessary torques for pitching and yawing, birds have a wide variety of tail shapes and sizes that allow them to perform agile manoeuvres such as perching [1][3]. Several studies have shown that the avian tail not only provides moments but also contributes to lift and reduces drag [2]. Furthermore, research into morphing avian tails in drones show important improvements in the manoeuvrability of the whole device [3], but no importance has been given to the shape of the tail.

This study is part of a project that aims at improving the flight performance of drones by studying birds. More precisely, the objective of this study is to find out how different shapes of avian-inspired tails affect the aerodynamic characteristics of drones. We will aim at

understanding how different tail shapes alter lift and drag. For this, three bird-like tails will be manufactured, as well as a fuselage that will act as the body of the bird (or the fuselage itself in case of a drone). These assemblies will be tested in a wind tunnel at different speeds and angles of attack to measure the forces they generate.

Chapter 2. TECHNOLOGY DESCRIPTION

During the development of this project, several technologies and industrial equipment will be used, most notably a 3-D printer, a laser cutter, a wind tunnel, a load cell and a robotic arm.

First, a 3-D printer is a machine that stacks very thin (about 0.17 – 0.25 mm) layers of material (plastic in our case) to produce a three-dimensional piece [25]. These pieces are designed in a CAD software (such as SolidWorks, the one that was used for the realisation of this project) and then exported into a "3-D object" file, that the printer can read. The main asset of this technology is the quality of the finished pieces, due to the very high precision of the machine, as well as the decent mechanical properties of the plastic used, which are more than enough for the objectives of this project.

Second, a laser cutter is a machine that uses a laser to cut sheets of material in two dimensions. The precision of this machine is also very high (in the order of a tenth of a millimetre) but can only produce two dimensional shapes. It can however, cut a wide range of materials.

Third, a wind tunnel is an array of fans that provide wind in the desired manner. Contrary to what one may think, the wind tunnel used for this project is not strictly a "tunnel", in the sense that it is not an enclosed space, but rather a group of fans that supply wind to whatever is placed in front of them. The wind tunnel used measures 1.94 x 1.74 metres and has 504 fans that can be set individually to supply a speed up to 11 m/s.

Fourth, a robotic arm is a machine often used in factories that can move in 6 different axes. The purpose of this machine is to accurately place an object in the desired place and orientation, being able to change its position smoothly. The robotic arm as well as the wind tunnel used in this project are shown in Figure 2.

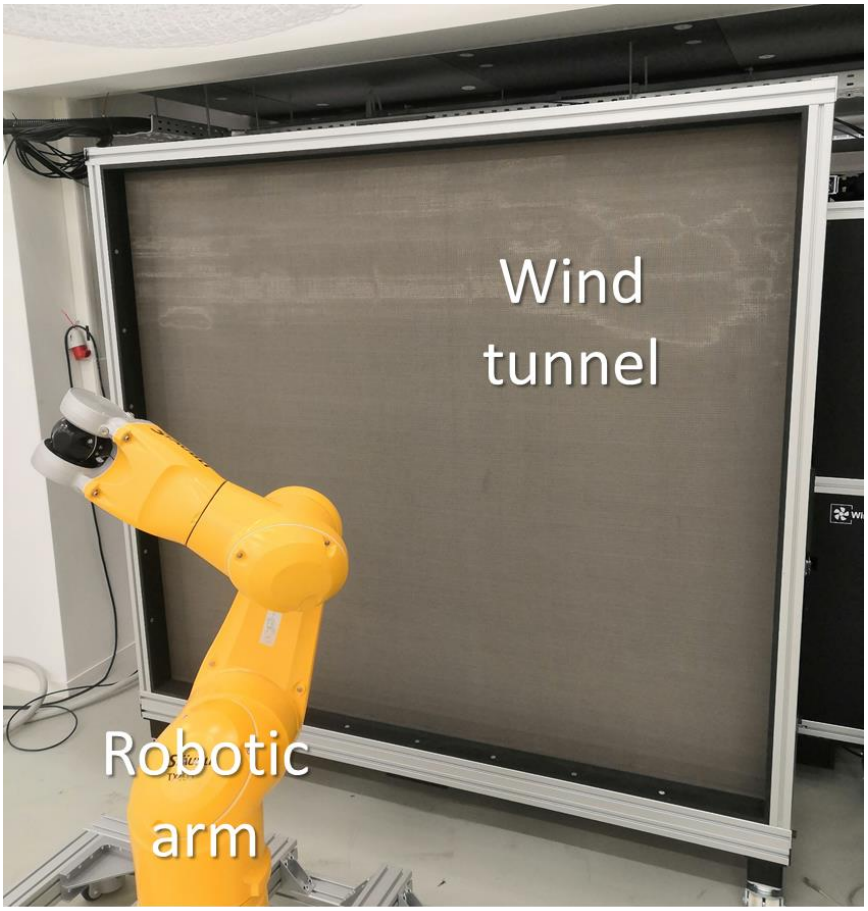

Figure 2. Wind tunnel and robotic arm.

In fifth place, a load cell is a small device (see Figure 3 below) that can measure forces and torques in all 3 axes. The data is gathered at a frequency of 1000 Hz and stored as a comma separated values (CSV) file.

Figure 3. Load cell ATI Nano17 with pen cap for scale.

Chapter 3. STATE OF THE ART

The aerodynamic performance of an airfoil is defined as its lift to drag ratio [4][5]; that is, the amount of drag it generates in comparison with the lift. Having said this, maximum lift and minimum drag are not necessarily the best option, as a high deceleration (meaning higher drag) is needed for landing, for instance. Classic aerodynamics tells us that lift and drag are proportional to the area of the airfoil [6], following the formulas:

$$L = \frac{1}{2} C_L S \rho v_\infty^2$$

$$D = \frac{1}{2} C_D S \rho v_\infty^2$$

Where S is the surface area of the airfoil, ρ is the density of the fluid (air in our case), v is the speed of the fluid relative to the airfoil and C is a coefficient (called lift – or drag – coefficient) that characterises the airfoil.

However, several authors that have studied the avian tail have come to different conclusion regarding the determination of lift and drag in tails. For instance, Thomas says that the (square of the) span of a bird tail is what determines the lift it generates, while the area determines the drag [4]. He goes further on to suggest optimal tail morphologies depending on the type of flight. For instance, he claims that the highest performance is achieved with a triangular tail spread at 120º and an aspect ratio of about 2.5. In another study in 1996, he mentions that the best lift to drag ratio is given by a high aspect ratio (the square of the span divided by the area) tail, backing up his initial theory [7].

In a more experimental approach, Maybury and Rayner performed tests in a wind tunnel that involved real (dead) birds, which had their wings removed and had successive trimmings in their tails. They measured the drag and found out that the more the tail was trimmed, the bigger the drag, hence concluding that the tail acts as a splitter plate, preventing the boundary layer from detaching from the animal and reducing the wake [2]. However, these

experiments were all carried out at 0º of angle of attack, so their validity when the bird soars at different angles is not certain.

We can see that there is no consensus on what parameters determine the performance of the avian tail. The authors do agree, however, that when studying the aerodynamics of a bird, one cannot sum up the independent effects of the body, wings and tail [2][7]. The airflow around each of these modifies the performance of the others.

Chapter 4. WORK DEFINITION

4.1 JUSTIFICATION

We have seen that the current drone market lacks a device that can be both agile and fast. Drones that sacrifice one of these capabilities are not well suited for tasks that encompass flight in cramped environments, like cities or forests. Society thus demands agile and fast drones because they can improve the quality of a wide range of missions, such as rescue, security or surveillance.

Where drones fail, birds excel, so it is a good idea to take inspiration from nature and see what exactly birds do that drones do not, in order to improve them. Looking at birds, the tail is an obvious tool they use in their advantage, as shown by the studies here mentioned. However, when studying the avian tail, there are two things authors do not seem to fully explain. These are the parameters that determine its performance and, more generally, the influence of the shape.

4.2 OBJECTIVE

Having said this, the main goal of this project is to understand how the shape of the tail affects the aerodynamics of the drone. This objective can be broken down into the following:

1. Choose several avian tail shapes found in nature.
2. Manufacture an appropriate testing setup to test the tails.
3. Measure the forces produced by the tails in different flight regimes.
4. Analyse the data.

4.3 METHODOLOGY

The way the project is to be carried out is the following. Firstly, several tails will be designed in order to compare their performance in flight. A fuselage will also be designed to host the several tails, mimicking a real bird or, more realistically, a drone.

With the dummy bird designed and manufactured, a testing setup will be constructed. Various auxiliary pieces will need to be designed and 3-D printed on order to hold the assembly together while in the wind tunnel tests.

Once the setup is ready, several wind tests will be carried out, varying the speed and the angle of attack of the different assemblies to test. These assemblies are the three tails with and without the fuselage, as well as the fuselage by itself.

The next stage will be the analysis of the results, that is, the calculation of the lift and drag in each situation and how the different parameters, such as the shape of the tail, the angle of attack or the wind speed affect them.

Finally, if time allows, several other tails will be designed and manufactured for testing. These tails will follow different design hypotheses than the ones used for the first tests and will enrich the study.

Chapter 5. DESIGN AND MANUFACTURING

In order to measure the aerodynamic effect of the wind on the several tail morphologies, a dummy bird was constructed, where the several tails could be attached for testing. Inspiration was taken from a rock dove, and its length scale was copied.

As seen in Figure 4, the rock dove has a body length of about 21 cm, and a circular tail with an angle of spread of roughly 120º and 10 cm of feather length. From here, a fuselage and several tails were manufactured, but no wings were attached. In spite of several authors mentioning that the study of the aerodynamics of a bird cannot be broken down to the study of the body, the wings and the tail; no wings were added to the prototype because they would make the study of the airflow around the tail too complex. Special care would have had to be put into the design and performance of the wings, as they inevitably provide lift and other torques to the bird (in fact they are the primary source of these). The correct approach to the wings would have taken too much time and would have lured the focus away from the tail, which is the main point of this project.

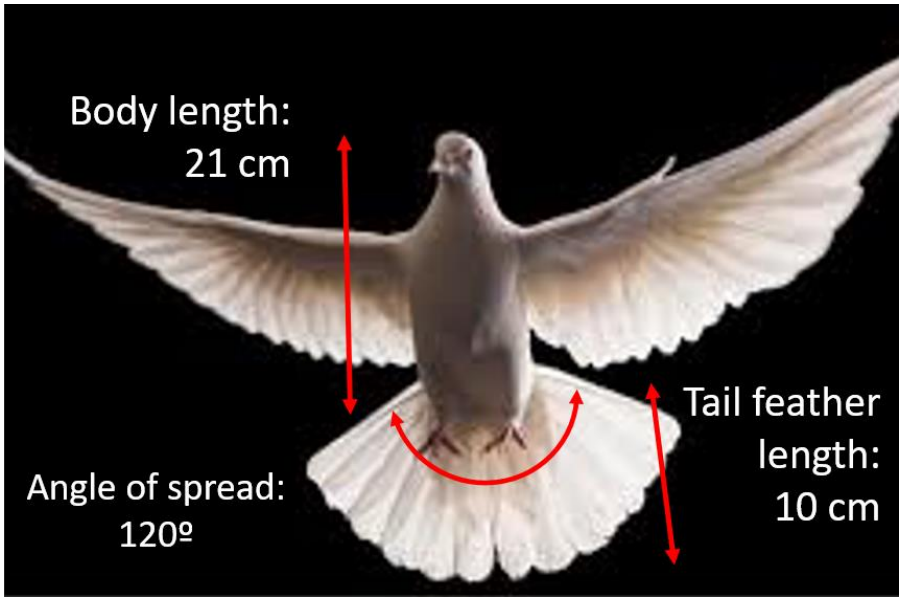

Figure 4. Measures of a regular rock dove [1].

5.1 TAIL DESIGN

For this study, three basic tail shapes were selected, often found in nature. These are a circular one (the original from the rock dove), a triangular one and a forked one, as displayed in Figure 5. The shapes these translate to are shown in Figure 6.

Figure 5. Three different tail shapes found in nature. Circular (dove) [9], triangular (red kite) [10] and forked (swallowed-tail kite) [11].

Figure 6. Shapes used for the actual design of the tails.

The main design constraint was that they must have the same Reynolds number when flying at a particular wind speed. As the reader may know, the Reynolds number characterises the flow of fluid around (or through) an object and is given by

$$Re = \frac{\rho * v * L}{\mu}$$

where L is the characteristic length of the object.

According to many authors [12][13][14], the length that best characterises an airfoil is the mean aerodynamic chord (MAC). This number indicates the mean distance between the leading and trailing edges of an airfoil and follows the formula:

$$MAC = \frac{2}{S}\int_0^{b/2} c(y)^2 dy$$

Where *S* is the surface of the airfoil, *b* its span and *c(y)* the chord at each coordinate y along the span.

Furthermore, to make the tails fit smoothly in the fuselage, they were all designed with an angle of spread of 110º. The choice of this value instead of the 120º is due to the fact that 120º made the two tails that do not correspond to the rock dove (triangular and forked) significantly bigger. Birds can, of course, furl the tail and reduce the angle of spread, and as 110 is very close to 120, we settled with this value. Having set these two magnitudes (angle of spread α and MAC), we have the following degrees of freedom and their effect on the MAC:

- Circular tail: 1 degree of freedom (span L)
  - L and MAC are directly proportional.
- Triangular tail: 1 degree of freedom (L).
  - L and MAC are directly proportional.
- Forked tail: 2 degrees of freedom (L and aspect ratio AR).
  - L and MAC are directly proportional.
  - AR and MAC are directly proportional.

A MATLAB script (tail_shapes.m) was written to speed up the design. This way, one can tune the different parameters and get the geometrical characteristics of the several tails, as well as the figures that show the top view.

A regular tail of a rock dove has a MAC of 79 mm, so the other tails were designed to exactly match this number. The triangular and forked tails face the problem of having very short chord in the vicinity of their lateral edges. This implies that in order to achieve the same

MAC as the circular shape, the tails would have had to be considerably larger. For this reason, an edge chord of 35 mm was added to the design. This slightly changes the relations between the degrees of freedom and the MAC shown before, but the main concept remains (increasing the span will certainly increase the mean aerodynamic chord). The few degrees of freedom were tuned so the tails would have a reasonable size, as they would have to be mounted on the fuselage. The final tail designs as well as their different characteristics are shown in Figure 7 and Table 1.

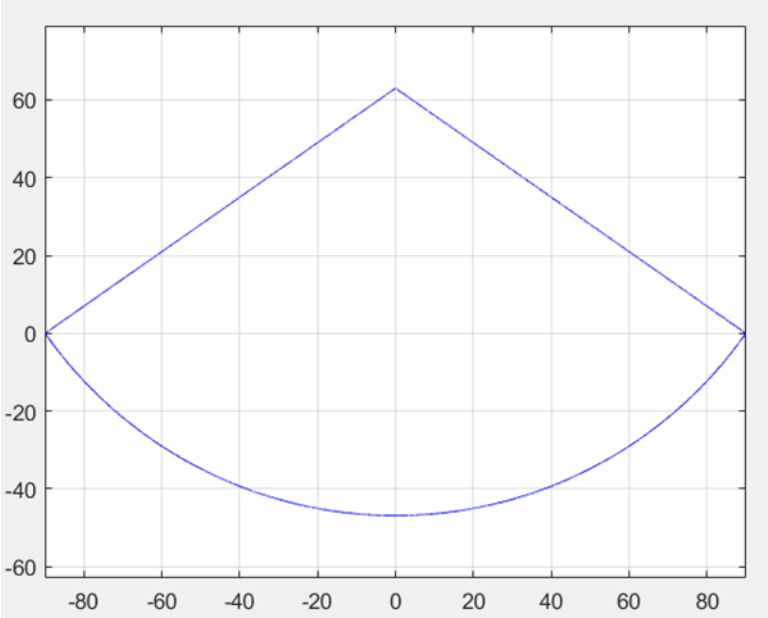

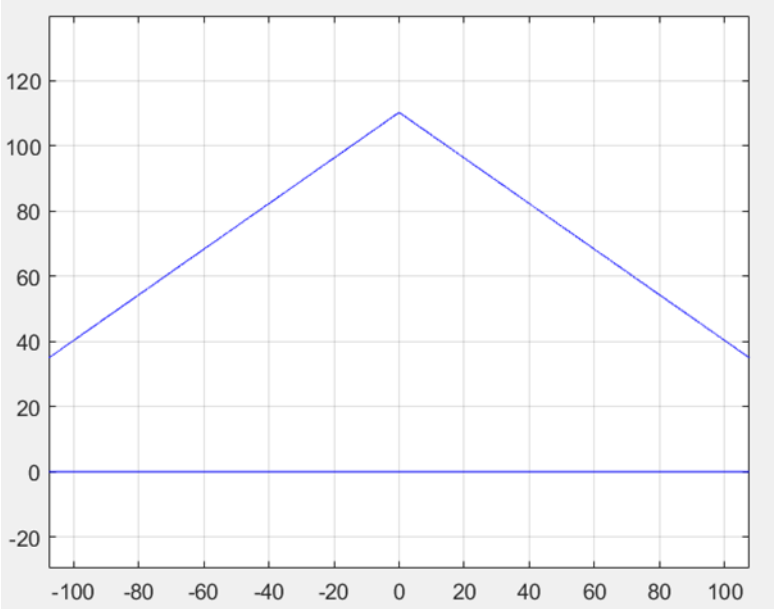

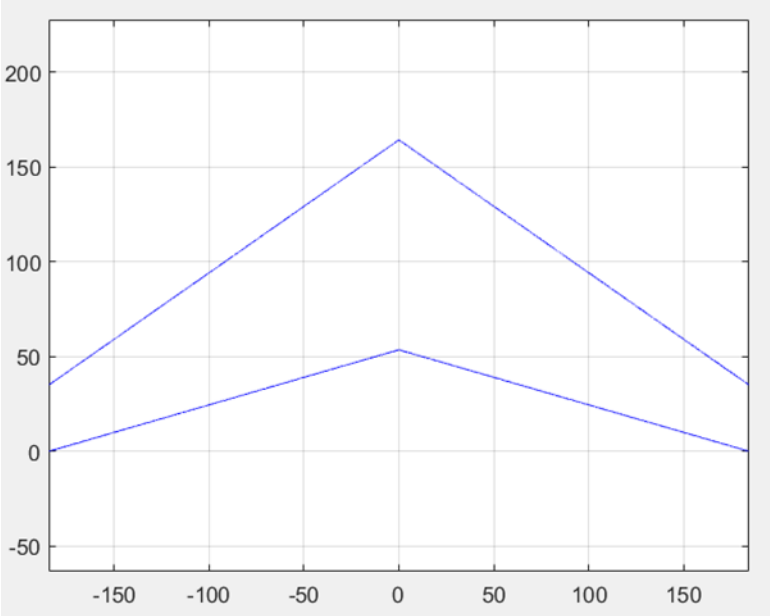

Figure 7. Final design outline of the tails (circular, triangular and forked)

	Circular	**Triangular**	**Forked**
MAC (mm)	79	79	79
Span (mm)	180	215	369

Area (mm^2)	11588	15617	26882
Aspect ratio (-)	2.8	3.0	5.1

Table 1. Characteristics of the designed tails

Having done this, the only thing remaining is to devise some sort of attachment to the different testing setups. The easiest way is to include holes for screws. Three non-aligned screws will suffice to hold the tail in place with the fuselage and be able to transmit pitching and rolling torques. A fourth screw was added, in line with the tails' vertex, as shown in Figure 8 to allow fastening between the tail and a small support used to test the tails by themselves in the wind tunnel. The choice of not adding a third screw (and hence transmit rolling torques) was to prioritise a small attachment that would cause the smallest perturbation of the airflow, knowing that the rolling torque created by the wind is theoretically zero due to the tails' longitudinal symmetry.

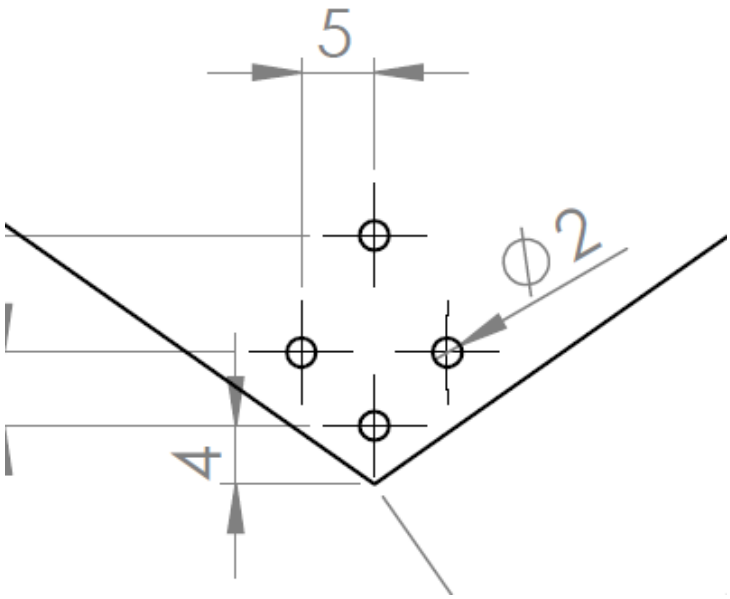

Figure 8. Fastening holes in tail.

5.2 FUSELAGE DESIGN

The fuselage will hold the tails in place and act as the body of the bird or, in a more realistic way, be the fuselage of a future drone, that will host all the circuitry.

The shape of the fuselage follows a revolution of a NACA 0025 airfoil profile, shown in Figure 9. This shape is easy to manufacture and aerodynamically reliable, as well as it does not differ too much from the actual shape of a rock dove. From here, several slots were included for the attachment of pieces. Firstly, a 3 mm groove was created at the trailing edge to insert the several tails. The groove opens at 110º allowing for a perfect fit of the tail. Furthermore, 3 holes were made to join the tails and the fuselage with screws, following the pattern described in Figure 8. Secondly, a circular hole was created, perpendicular to the longitudinal axis, to allow a rod to hold the fuselage in place. This rod (if it were infinitely long) passes through the centre of mass of the fuselage, so it can stand upright if we attach a small base to the low end of the rod. Finally, the whole piece was made hollow, with a thickness of 4 mm to lower the mass and save material. The technical drawing of the fuselage, as well as of all the tails can be found in ANNEX III. Technical drawings.

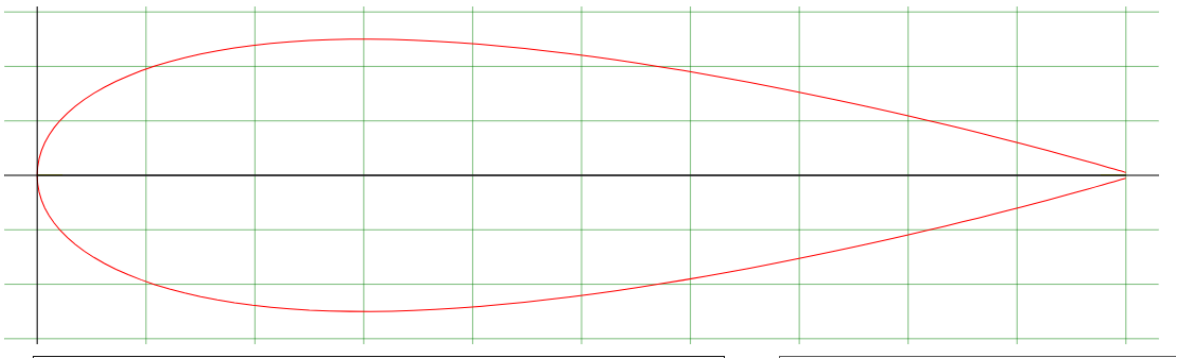

Figure 9. NACA 0025 profile [15].

5.3 MANUFACTURING

The tails were manufactured out of 3 mm FDM (plywood) and cut with a laser cutter. This material is very smooth, so only the leading edges were sanded. The final manufactured circular tail is shown in Figure 10.

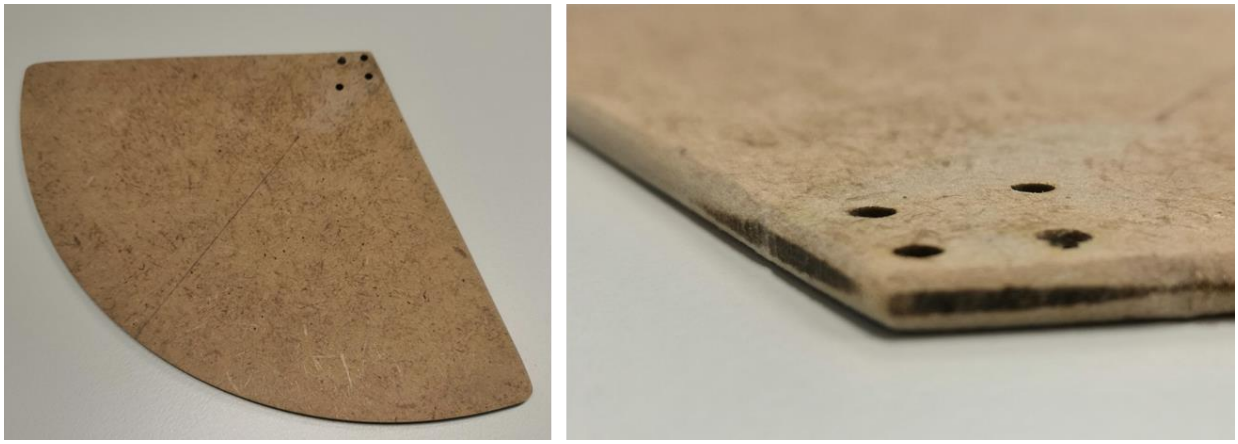

Figure 10. Manufactured circular tail.

The fuselage was manufactured out of ABS thermoplastic with a 3D printer in two pieces for faster printing. These pieces were then joint together with a two-component epoxy glue and their surfaces sanded until the fuselage resembled one continuous smooth piece of plastic. Finally, the necessary holes were threaded. Note that these holes were printed with a slightly smaller diameter so when tapped, they would result in the desired metric.

5.4 ASSEMBLY

Apart from the tails and the fuselage, other pieces are needed to perform the tests in the wind tunnel and keep the objects together. The conceived testing setup for the fuselage with a tail is shown in Figure 11.

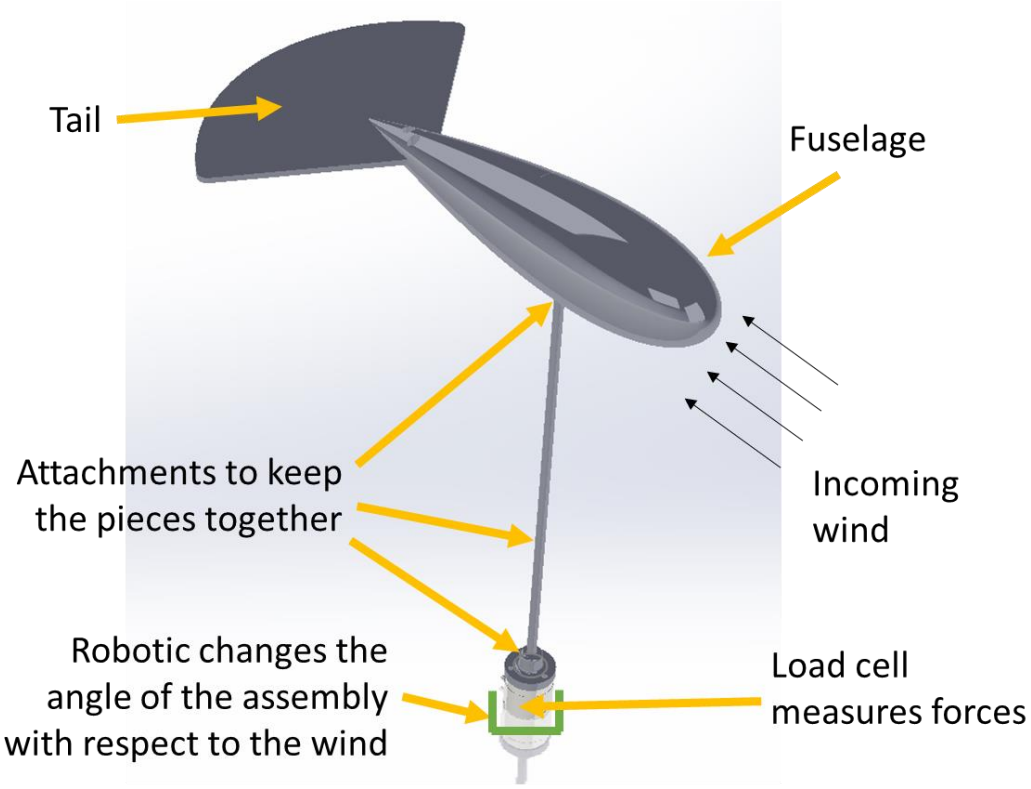

Figure 11. Conceived testing setup.

These pieces encompass a 27 cm metal rod that connects the body subject to the tests with the load cell and several other 3-D printed pieces that hold the assembly together. These are very simple pieces that will not be discussed here, a view of them can be found in ANNEX III. Technical drawings.

Chapter 6. TESTING

With the fuselage and the several tails, the testing setups shown in Figure 12 were constructed.

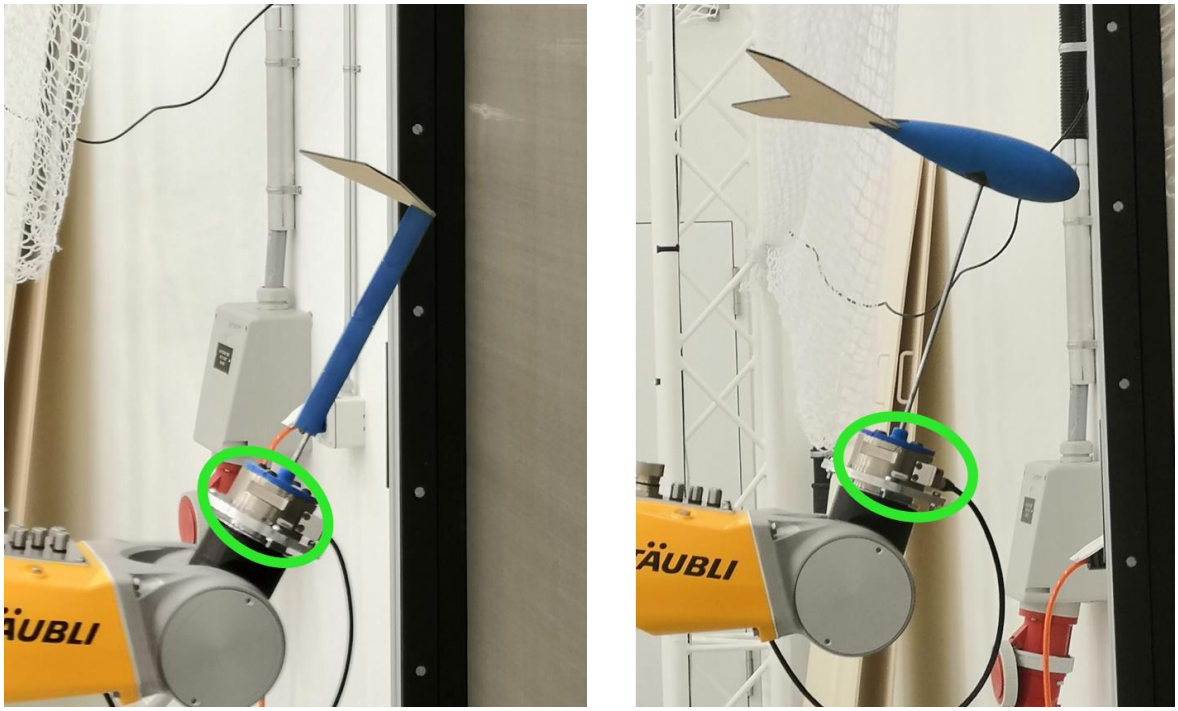

Figure 12. Actual testing setups for just the tails (left) and fuselage + tail configurations (right). The load cell is highlighted in green.

A metal rod connects the load cell with the dummy bird. The robotic arm changes the angle of attack of the whole assembly with respect to the freestream wind, provided by the wind tunnel. Seven assemblies were tested: the fuselage by itself, the 3 tails by themselves and the fuselage with each of the several tails.

For a smooth plate, such the tails at hand, the transition from laminar to turbulent flow occurs at a Reynolds number of $Re_c = 3 \cdot 10^6$. The mean aerodynamic chord of all three tails being 79 mm, we have

$$v_c = \frac{Re_c * \mu}{\rho * L} = \frac{3 \cdot 10^6 * 18.13 \cdot 10^{-6}}{1.2041 * 0.0079} = 572\ m/s$$

The maximum flying speed of a pigeon varies considerably from source to source [16][17][18][19], but it is within 60 km/h (16.7 m/s) and 150 km/h (41.7 m/s), so the flow around the tails will always be laminar, no matter the position along the tail.

In order to achieve a good balance between number of measurements and time consumed, the objects were tested between 0 and 45 degrees in steps of 5 degrees and between 0 and 10 m/s (the maximum wind speed that the wind tunnel can provide is 11 m/s) in steps of 2 m/s. Only negative angles of attack were tested (meaning the front is closer to the ground than the rear) because the bird is symmetrical with respect to a horizontal plane, generating no lift if parallel to the ground (0° angle of attack). Therefore, the drag in the same at 10° and negative 10°, while the lift changes sign.

The testing procedure is as follows: once the assembly is firmly placed on the robotic arm, the fans are turned on to generate wind at a particular speed. The robot then waits 25 seconds to change the angle of the assembly. The test proceeds by waiting 10 seconds between each change in angle. Thus, 10 seconds after an angle of 45º is reached, the fans are brought to a halt and the robot places the assembly at 0º. The process is repeated for all 6 wind speeds and for each of the 7 assemblies.

Throughout this process there is an ATI Industrial Automation Gamma load cell [20] sampling the forces and torques in each of the 3 axes at a rate of 1000 Hz, averaging over 16 samples, thus outputting about 63 samples per second. At the beginning of each run at a particular wind speed, the load cell was biased, so the instant before the fans were connected, it read 0 in all 6 magnitudes.

One should notice that the load cell moves with the robot, so the forces and torques are not referenced to the ground except at an angle of attack of 0°. To get the force the wind exerts on each assembly at a particular wind speed and angle of attach, 2 seconds of samples are taken (about 120 measurements), corresponding to the last 2 seconds before the angle of

attack is modified. This way steady airflow around the object of study is guaranteed. These forces (and torques) are then projected on to still axis on the ground in the following manner:

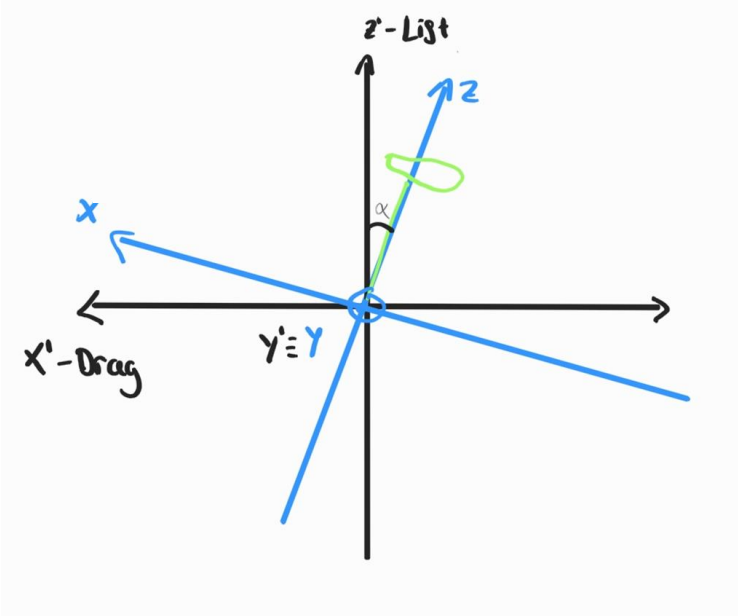

Figure 13. Transformation of magnitudes between moving assembly (blue) and ground (black).

$$F_x' = F_x * cos(\alpha) - F_z * sin(\alpha)$$
$$F_y' = F_y \quad (1$$
$$F_z' = F_x * sin(\alpha) + F_z * cos(\alpha)$$

The forces on the tail are calculated as follows:

$$F_{tail,wind} = F_{assembly,wind} - F_{assembly,no\ wind} - \left(F_{support,wind} - F_{support,no\ wind}\right) \quad (2$$

Where F is either the lift or the drag. The support encompasses everything that is placed on top of the load cell but the tail itself, that is, the fuselage and all its attachments for the fuselage and tail configurations, or the piece that holds the tail in place when the tail is being tested on its own.

Having performed the tests, several MATLAB scripts were used to sort and analyse the data. Most notably, file main.m allows a first visualisation of the data and file ExportDataArrays.m performs the calculations indicated above and exports these data in

matrices that will later be used to analyse the forces. These files can be found in ANNEX I. Source code.

However, once the results were analysed (these are briefly discussed in the next chapter), we found that they were somehow unreliable and therefore decided to repeat the tests with a different strategy. This new approach is very similar to the one described above, but some changes were made.

Firstly, a new load cell with higher resolution was used. Table 2 shows the characteristics of the load cell used in the previous experiments (Gamma), while Table 3 shows the same for the newer ones (Nano17). The resolution is notably better but the sensing ranges are also considerably reduced, which can pose a problem.

Calibration	Fx,Fy	Fz	Tx,Ty	Tz	Fx,Fy	Fz	Tx,Ty	Tz
SI-32-2.5	32 N	100 N	2.5 Nm	2.5 Nm	1/160 N	1/80 N	1/2000 Nm	1/2000 Nm
SI-65-5	65 N	200 N	5 Nm	5 Nm	1/80 N	1/40 N	10/13333 Nm	10/13333 Nm
SI-130-10	130 N	400 N	10 Nm	10 Nm	1/40 N	1/20 N	1/800 Nm	1/800 Nm
	SENSING RANGES				RESOLUTION			

Table 2. Gamma load cell characteristics [20].

Calibration	Fx,Fy	Fz	Tx,Ty	Tz	Fx,Fy	Fz	Tx,Ty	Tz
SI-12-0.12	12 N	17 N	120 Nmm	120 Nmm	1/320 N	1/320 N	1/64 Nmm	1/64 Nmm
SI-25-0.25	25 N	35 N	250 Nmm	250 Nmm	1/160 N	1/160 N	1/32 Nmm	1/32 Nmm
SI-50-0.5	50 N	70 N	500 Nmm	500 Nmm	1/80 N	1/80 N	1/16 Nmm	1/16 Nmm
	SENSING RANGES				RESOLUTION			

Table 3. Nano17 load cell characteristics [21].

Secondly, the rod connecting the load cell to the assembly was cut to reduce the torque on the Y axis, which has a maximum sensing range of 120 Nmm. This maximum sensing range means that, if exceeded, the readings become unreliable, although the device itself will not break; permanent damage toccurs with a much higher load. We arrived at the conclusion that, by halving the metal rod, safe and reliable tests could be performed with the new load cell.

	+ T_y (Nmm)			-T_y (Nmm)		
	Maximum read value	Maximum steady-state value	New setup approximation	Maximum read value	Maximum steady-state value	New setup approximation
Just circular	124	22	27	148	118	43
Just triangular	104	25	38	180	142	46
Just forked	117	41	78	279	203	45
Fuselage	167	27	14	374	233	117
Fuselage + circular	245	43	60	353	301	113
Fuselage + triangular	169	45	78	362	328	109
Fuselage + forked	229	80	148	453	399	92

Table 4 shows the comparison between several torques in the Y axis used to reach this conclusion. Highlighted in blue we have the maximum recorded values during the test. Values in the -T_y column occur when there is no wind, whereas the values in the +T_y column occur at maximum wind and low angles of attack. In black, maximum values during the steady state. We can indeed surpass the threshold of 120 Nmm during the transient, as the magnitudes recorded here are not used. To calculate the values during steady state, a low-pass filter was applied to the original data, with a cut-off frequency of 0.5 Hz that removes most of the noise and vibrations, hence given a conservative estimate of the maximum torque in the steady-state. This is shown in Figure 14. The green column corresponds to an approximation of the maximum Y torque for the new setup (once the rod is halved). This approximation is calculated by taking the maximum steady-state torque and adding the torque of each assembly at 0º and no wind, removing the offset produced when the load cell is biased at the beginning of each run. The calculations yield that only in one case the sensing range is surpassed.

Torque / Assembly tested	+ T_y (Nmm)			-T_y (Nmm)		
	Maximum read value	Maximum steady-state value	New setup approximation	Maximum read value	Maximum steady-state value	New setup approximation
Just circular	124	22	27	148	118	43
Just triangular	104	25	38	180	142	46
Just forked	117	41	78	279	203	45
Fuselage	167	27	14	374	233	117
Fuselage + circular	245	43	60	353	301	113
Fuselage + triangular	169	45	78	362	328	109
Fuselage + forked	229	80	148	453	399	92

Table 4. Comparison between maximum Y torques during first round of tests (encompassing all wind speeds and angles of attack). Blue columns show maximum recorded values, purple columns show maximum recorded values during the steady state and green columns show the maximum approximated value for the next tests.

Thirdly, the testing procedure was changed. This time, the assembly to test was placed at a given angle of attack, then the load was cell biased and finally the fans were turned on, from 2 m/s to 10 m/s in steps of 2. This way the load cell only records the forces the wind exerts on each assembly at a given angle of attack, reducing the number of operands in (2) from four to two. Thus, to calculate the aerodynamic effect of the wind on the tails, we first have to project the same way explained in (1), but (2) becomes:

$$F_{tail,wind} = F_{assembly,wind} - F_{support,wind} \quad (3$$

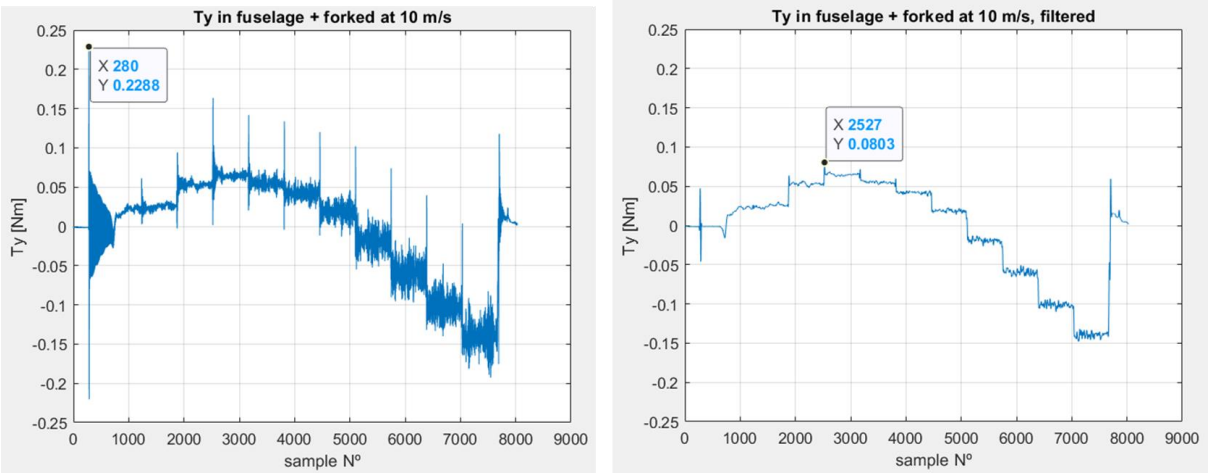

Figure 14. Measured Ty (left) and filtered (right).

Figure 15 shows the new setup for the second round of tests. Even though Table 4 shows that the torques applied to the new load cell would be withing the sensing limits, this was proved not to be the case. At some point while testing the fuselage + triangular tail and fuselage + forked tail assemblies, the 120 Nmm threshold was exceeded, and the measurements were clearly affected (see Figure 19 in Result analysis – Second round of tests). For this reason, these two assemblies were not tested fully.

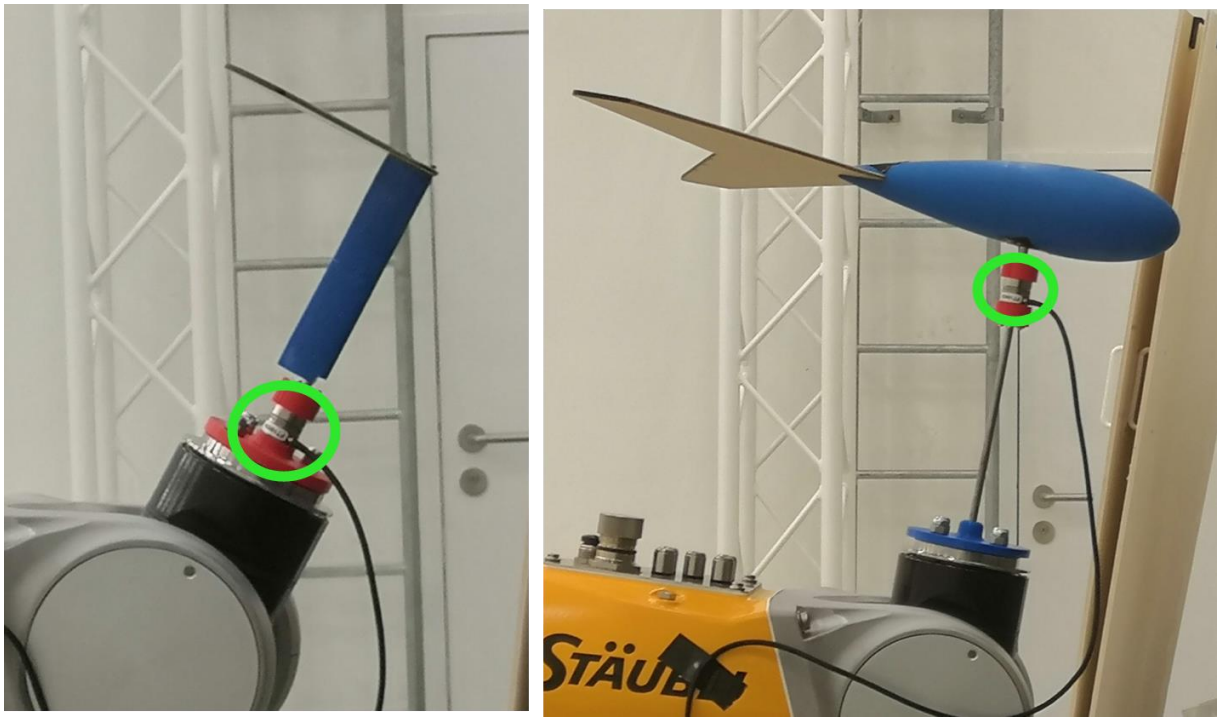

Figure 15. New testing setups for just the tails (left) and fuselage + tail configurations (right). The load cell is highlighted in green.

Chapter 7. RESULT ANALYSIS

7.1 FIRST ROUND OF TESTS

The first round of tests will be briefly presented here, as well as the reason why it was ruled out, followed by the proper results obtained during the second testing stage.

The following figures show the evolution of the lift and drag produced by the tails when mounted on the fuselage as a function of the angle of attack. There are some clear inconsistencies about these results. First, the standard deviation is considerably high, especially in the circular and triangular tail configurations. The measurements overlap with those of other wind speeds and angles of attack, so the trend in the mean values is not very reliable. Second, and perhaps more important, there are some results that seem impossible. The drag at 2 m/s is in most cases, completely below 0 N (up to -0.05 N), which is not possible, as the wind will always push back the objects that lie in its path. This probably has to do with the number of measurements (4 to be exact, as shown in (2)) that have been considered to produce these data. Adding 4 variables with noise (interpreted here as the standard deviation) implies that the noise of the sum is up to 4 times as great, decreasing the reliability of the measurements. Furthermore, the more measurements we add, the higher the likelihood of one of them being wrong, and hence the final sum as well. For these reasons we decided to rule out the results of this experiment and redo it with a new approach, as previously explained.

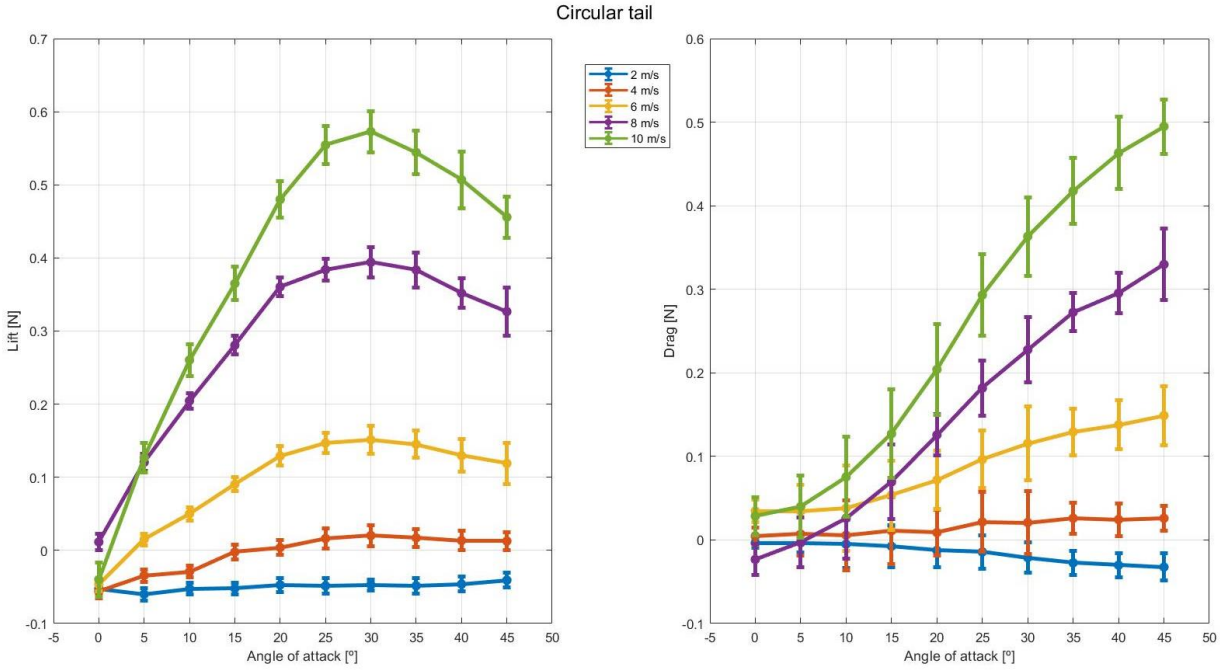

Figure 16. Lift and drag produced by the circular tail as a function of the angle of attack. Bars show ± standard deviation.

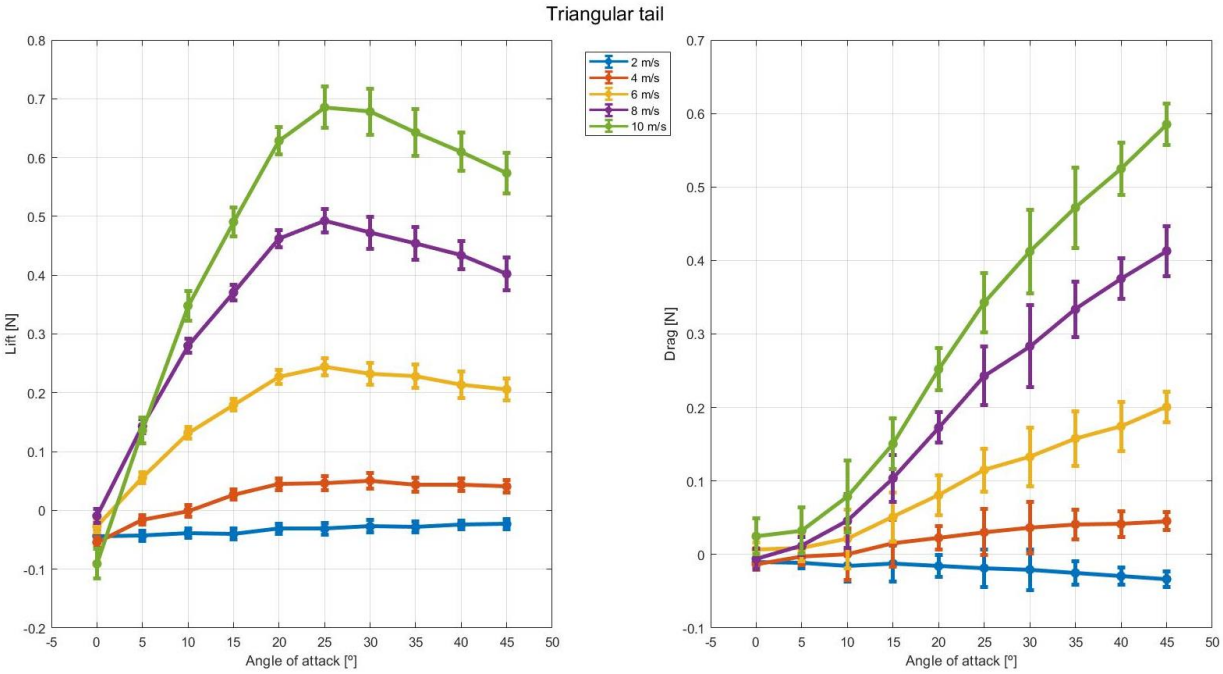

Figure 17. Lift and drag produced by the triangular tail as a function of the angle of attack. Bars show ± standard deviation.

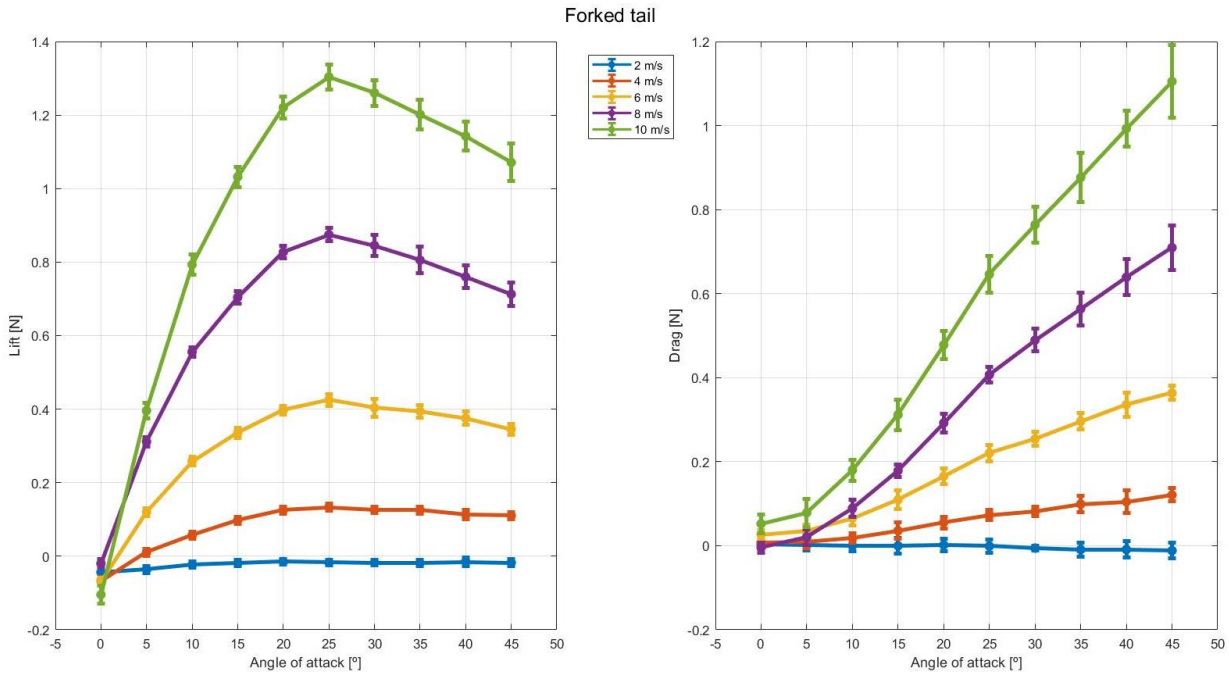

Figure 18. Lift and drag produced by the forked tail as a function of the angle of attack. Bars show ± standard deviation.

7.2 SECOND ROUND OF TESTS

The new tests showed clearer results, which will be presented here. However, due to the fact that the fuselage with the triangular and forked tails could not be tested fully, the data showed here corresponds to the tests where no fuselage was attached to the tails unless otherwise specified.

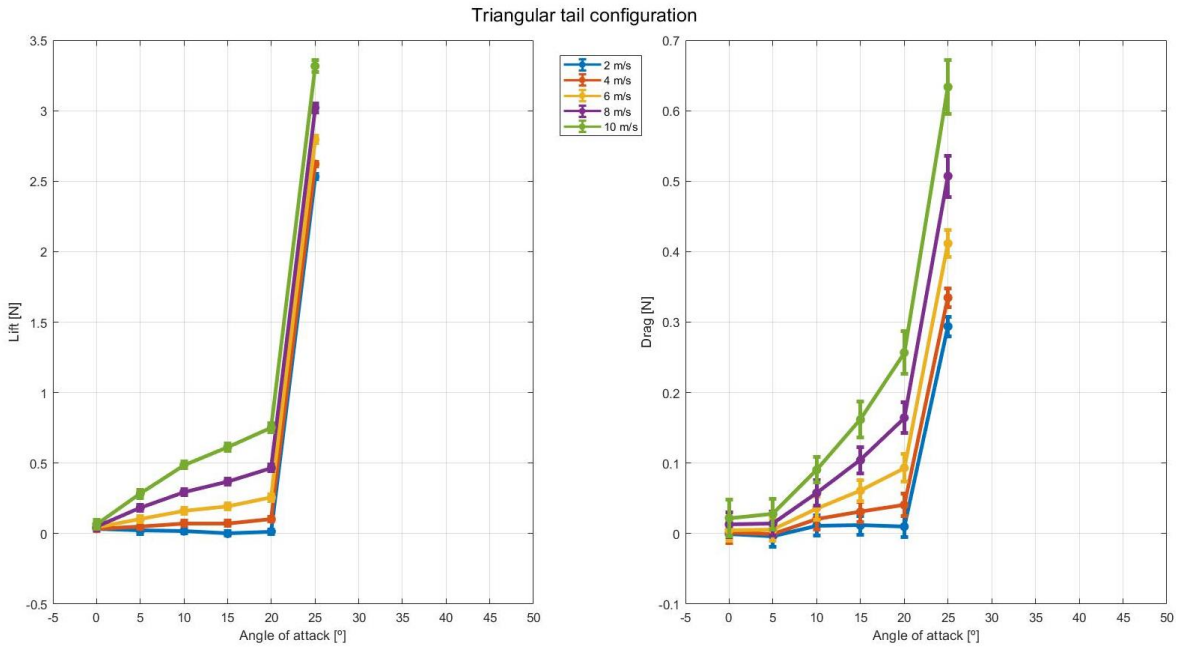

Figure 19. Forces on the tail for the fuselage + triangular tail assembly. Once the maximum torque in the Y axis is surpassed, (at about 20º), the measurements become clearly astray.

The first thing to consider is that, as shown in Figure 20Figure 23, the forces exerted by the wind at 2 and 4 m/s are small and encompass a high standard deviation, so they have been left out of the study. Furthermore, these figures show a negative lift at 0º of angle of attack. As the tails are completely flat, they should generate no lift when held horizontal; however, the extrapolation (lines) show that zero lift is achieved, for all tails and wind speeds, at about 2 or 3 degrees, leading us to conclude that there was a slight offset in the angle of attack while testing. Thus, the data has been modified accordingly (by shifting everything 3 degrees to the left).

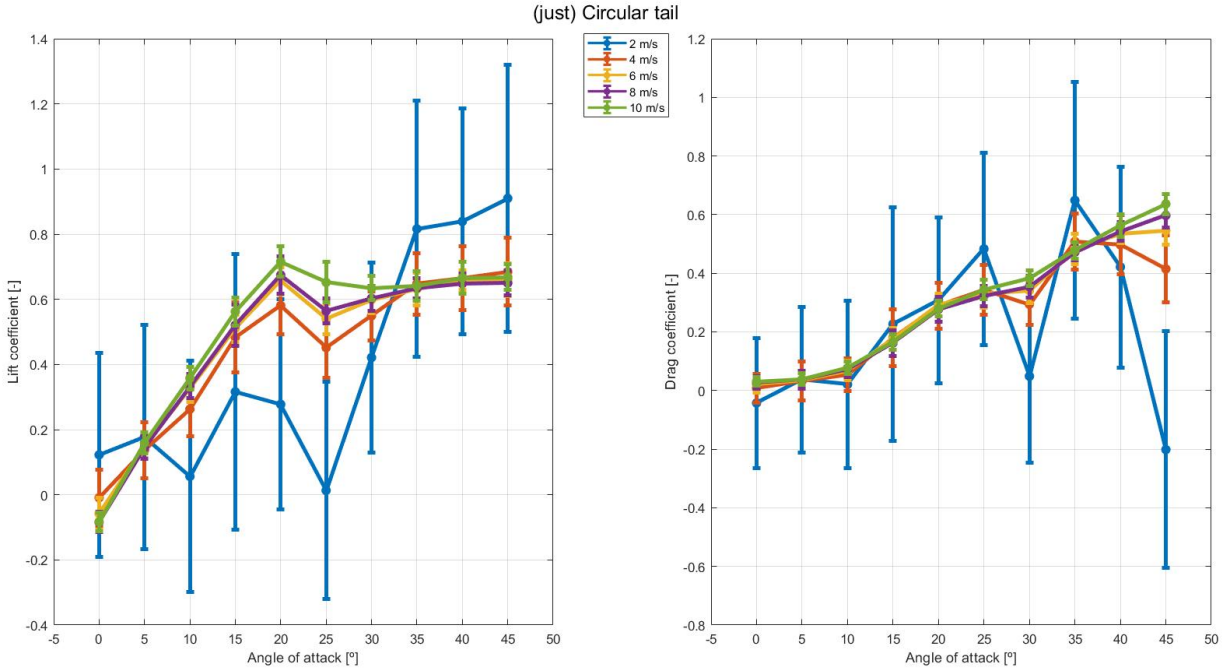

Figure 20. Lift and drag coefficients for the circular tail. Bars indicate ± standard deviation.

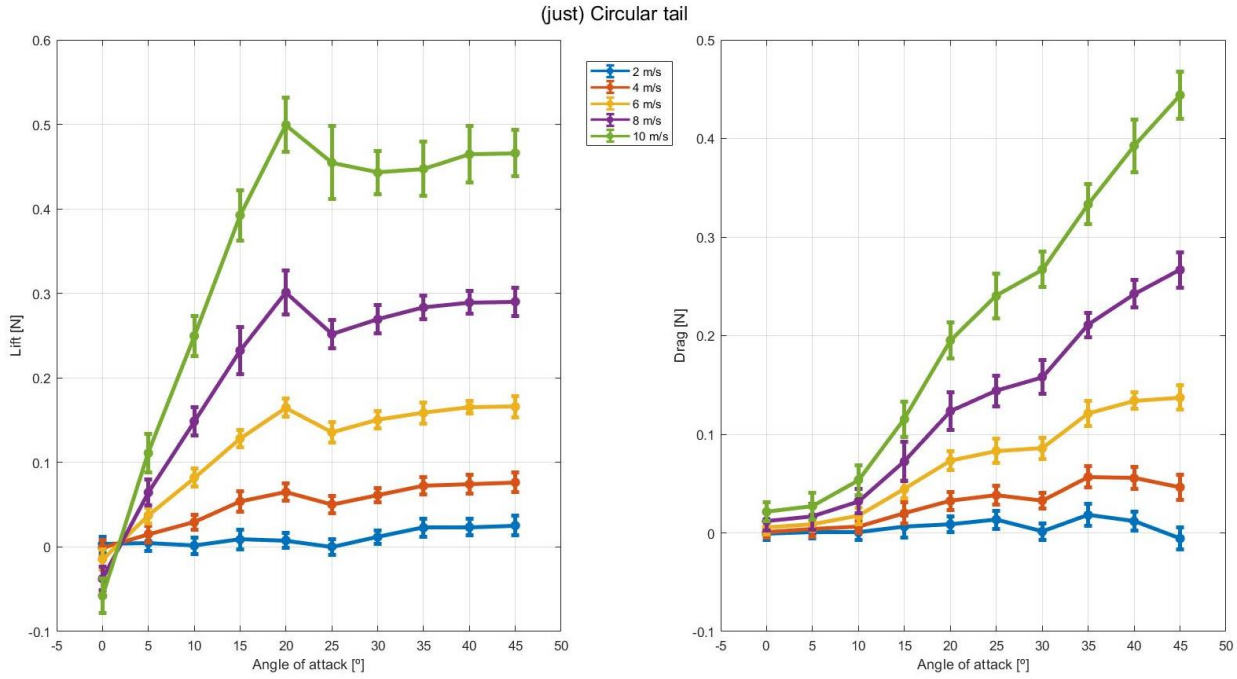

Figure 21. Forces on the circular tail. Bars indicate ± standard deviation.

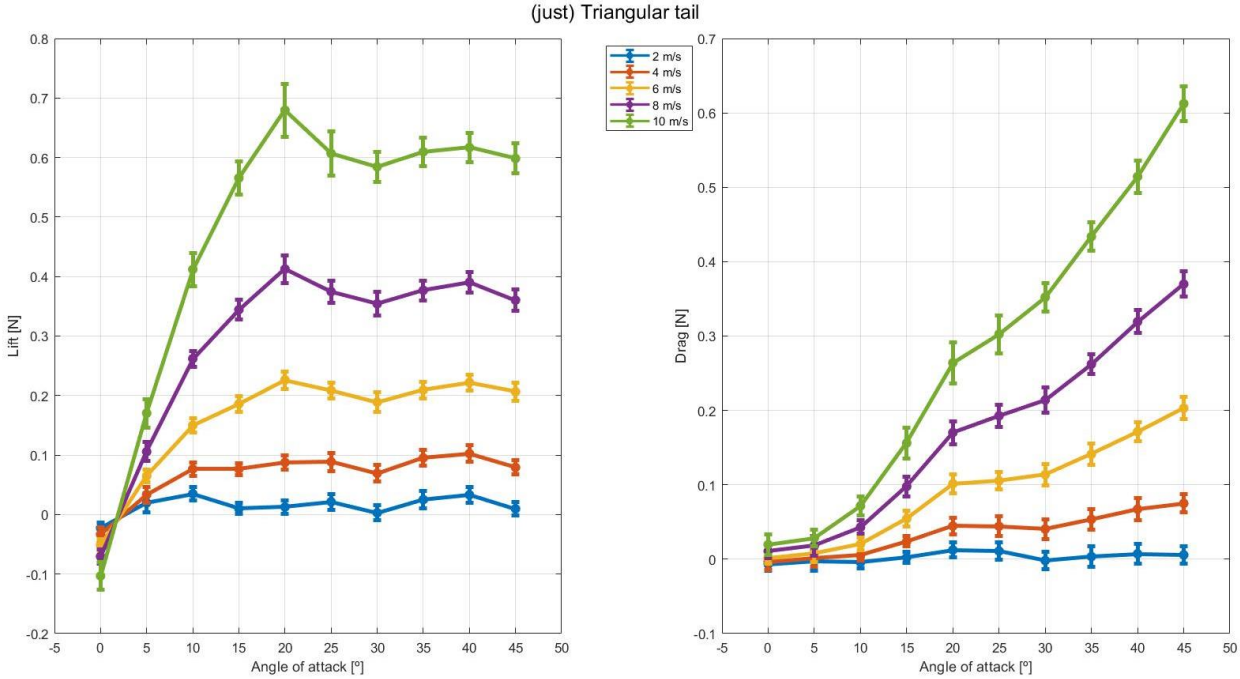

Figure 22. Forces on the triangular tail. Bars indicate ± standard deviation.

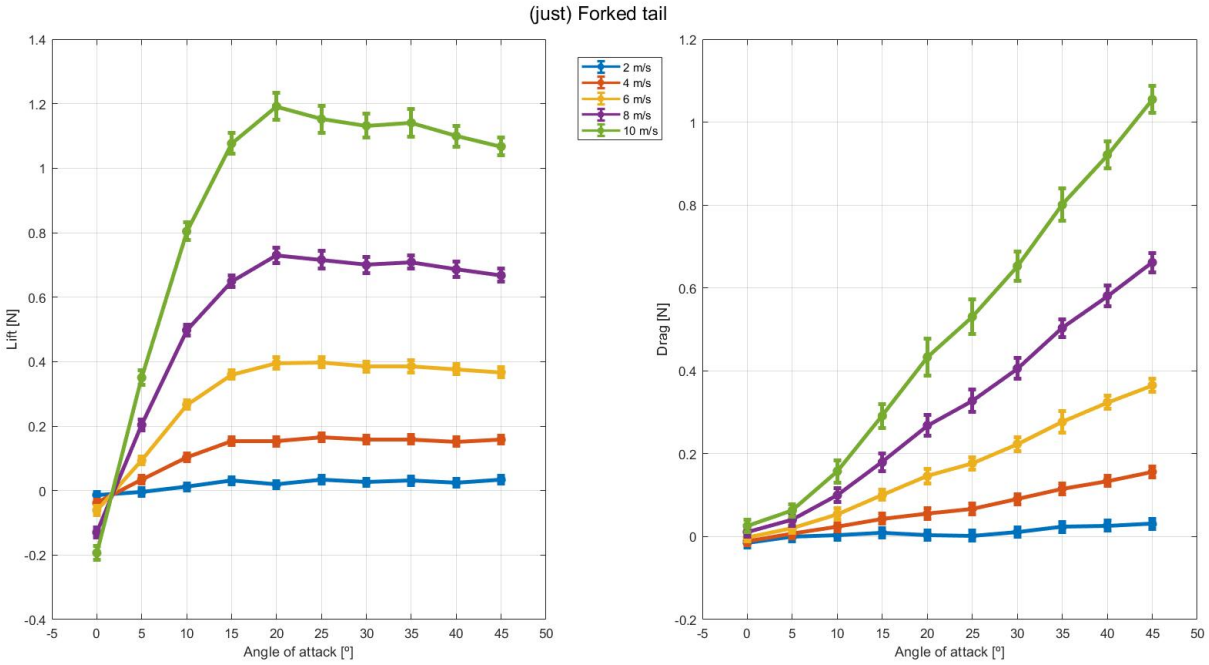

Figure 23. Forces on the forked tail. Bars indicate ± standard deviation.

Having said all this, the actual results with the final and adjusted data will be presented here.

Lift

As seen in Figure 24 and Figure 25, the most notable characteristic of the lift data is the stall angle, which happens between 20-25º for all tails. Having said this, the shape that generates the highest lift coefficient is the forked one, which generates up to 0.1 more lift than the other two just before stalling, although this value decreases with increasing speed.

Drag

We can see how the drag coefficient is independent from the shape of the tail and the speed at which it flies. The only parameter that describes its behaviour seems to be the angle of attack, where all shapes and speeds have a similar value, always within a 0.05 window.

Lift to drag ratio

In terms of lift to drag ratio, we can see in Figure 26 that at low angles of attack there are considerable differences, however, as we increase the angle, the ratio decreases for all tails and overlaps. For the low angles, the triangular tail offers greater lift to drag, up to 8 points more for 6 m/s, although this value decreases as the wind speed increases.

Influence of the fuselage

Figure 27 shows the lift and drag generated by the tail when we tested two different assemblies: the tail attached to the fuselage and the tail by itself. Although the data for both configurations follows similar patterns, when the fuselage is attached, the forces generated are considerably higher (up to 40%) when the angle of attack surpasses 20º (stalling angle).

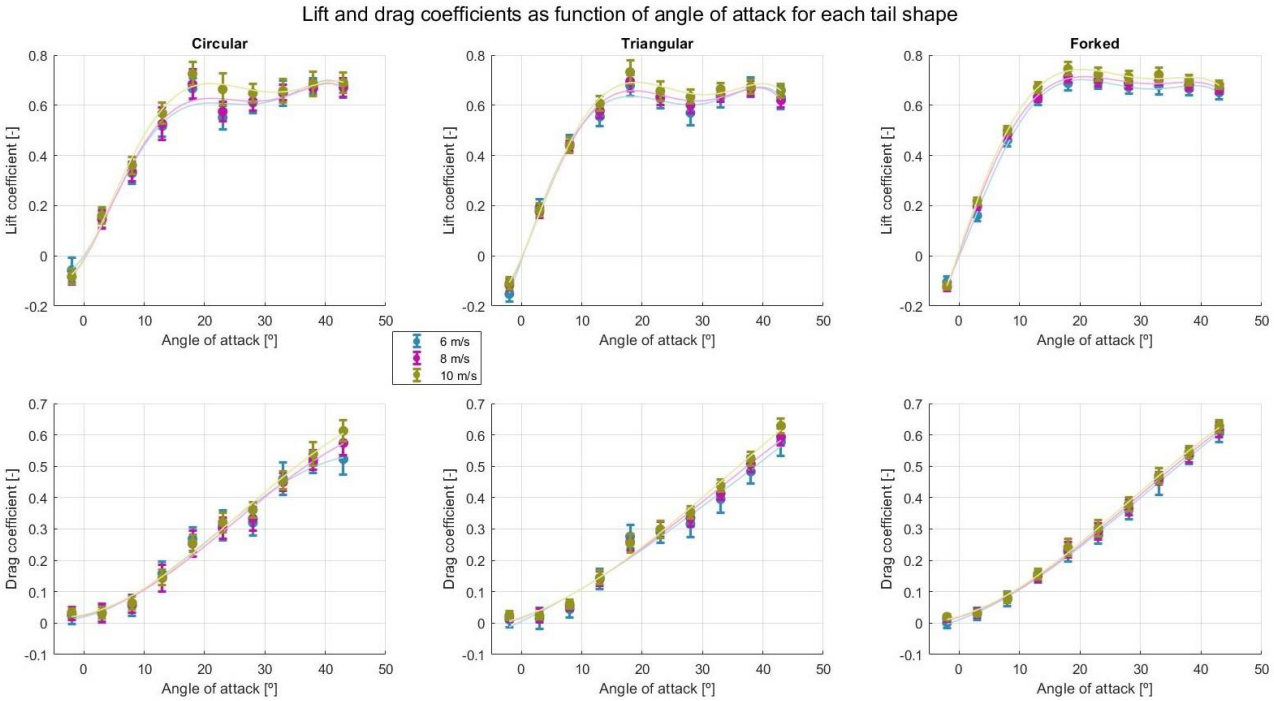

Figure 24. Lift and drag coefficients of the 3 tails. Bars show standard deviation.

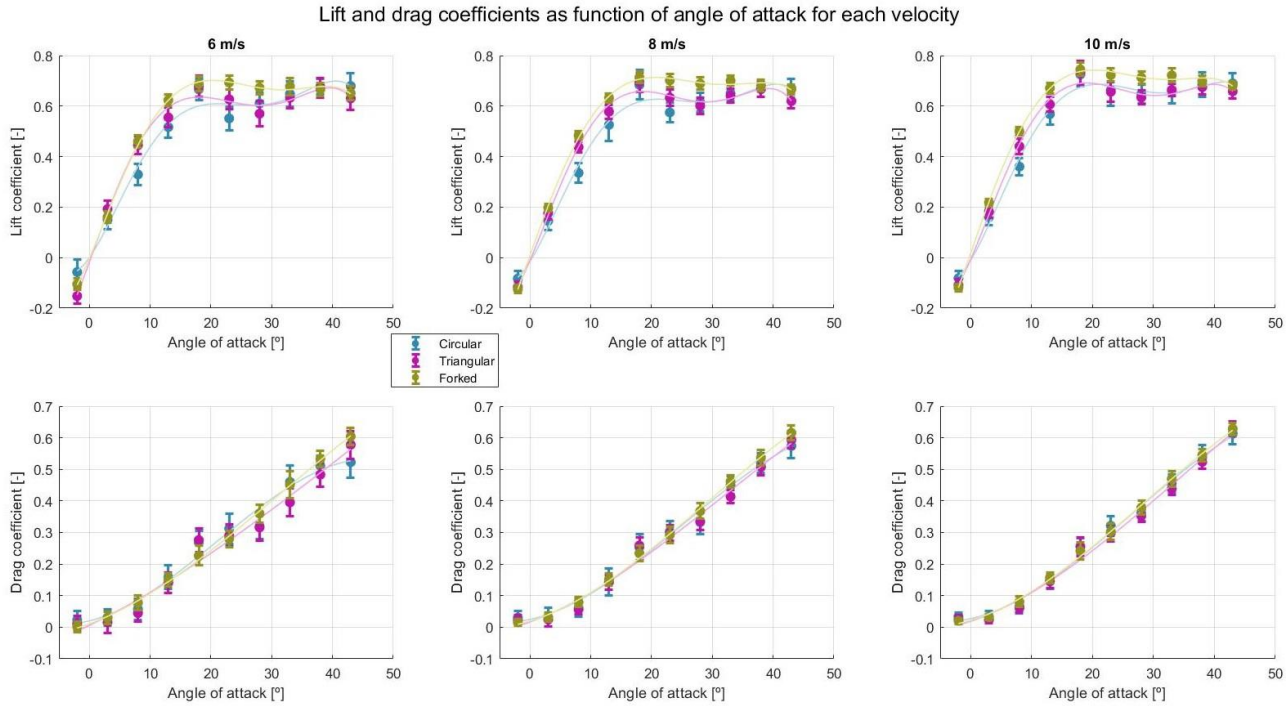

Figure 25. Lift and drag coefficients of the 3 tails. Bars show standard deviation.

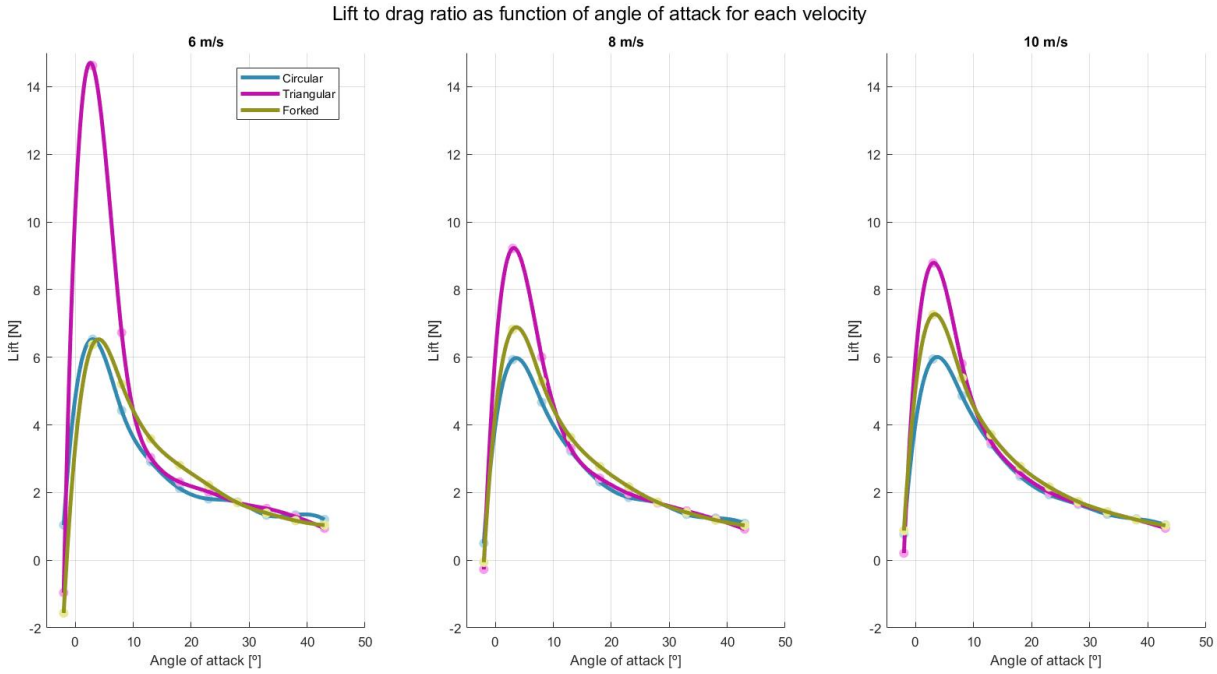

Figure 26. Lift to drag ratio of the 3 tails.

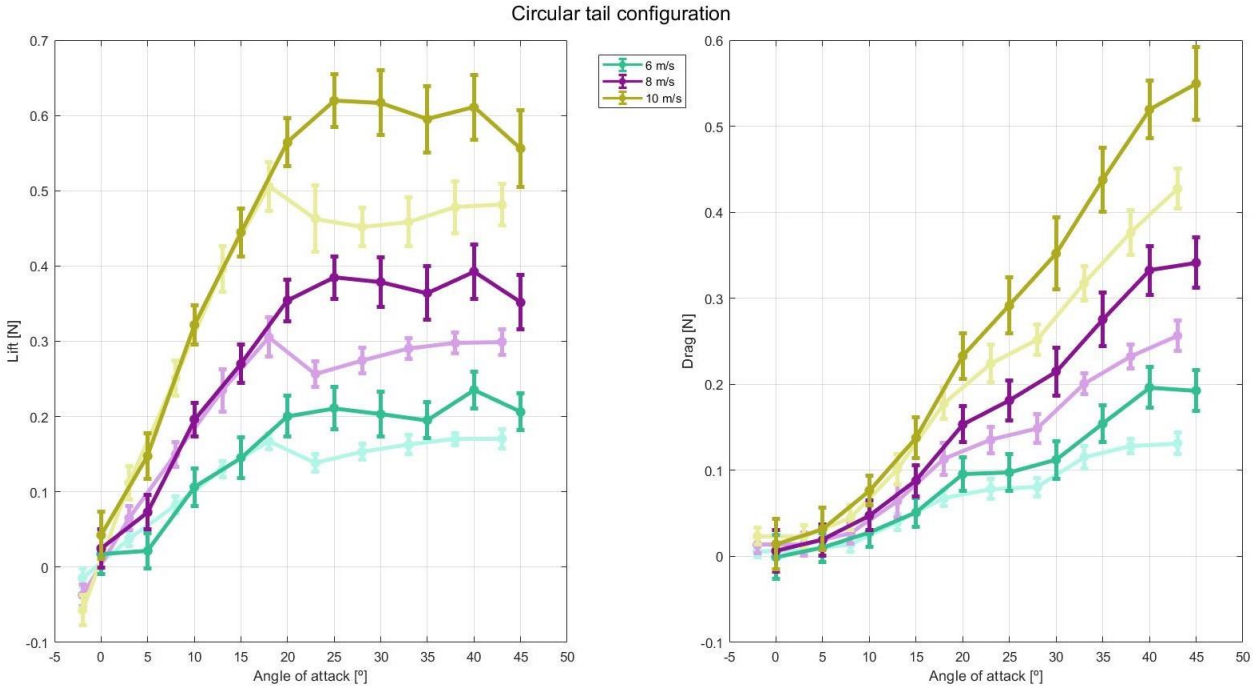

Figure 27. Aerodynamics of the tail for the two assemblies that encompass the circular tail. Strong colours correspond to the fuselage-tail assembly, while faint ones correspond to the tail by itself. Bars show standard deviation.

Chapter 8. DISCUSSION AND FUTURE WORK

The studies performed here have led us to the following conclusions.

First, contrary to what Thomas says [7], the best lift to drag ratio is not given by a high aspect ratio wing (tail, in our case). We have found out that, with matching Reynolds number, the best lift to drag ratio is achieved with a triangular tail, this one having a substantially lower aspect ratio than our forked tail (see Table 1). Hence, the triangular tail offers a higher performance when flying at low angles of attack, which would be the optimal solution if the aim of our drone were to cover distance without aggressive manoeuvring, as a low angle of attack also means low forces. This approaches the conclusion reached by Thomas (see Introduction) on the highest performant tail, although in his definition of performance he also included the moment arm of the forces generated by the tail. On the other hand, if we are interested in a fast deceleration (landing), the shape of the tail does not play a significant role, as the tail would likely be set at a high angle of attack to increase drag and here all the tails have similar performance.

Second, in terms of pure lift, the forked tail offers, at any given speed, a higher lift coefficient than the other two tails (see Figure 25). This is probably due to the considerably higher aspect ratio of this tail in comparison with the others, that have somehow similar aspect ratios and hence offer similar lift coefficients, although slightly higher for the forked tail, whose aspect ratio is greater than that of the circular one. The stall angle for our tails is slightly smaller than what other delta wing theories and experiments suggest (in the vicinity of 30º) [22][23][6]. However, these wings have angles of spread that are much lower than the 110º used in our experiments.

Third, as stated by Thomas and Maybury et al., the body of the bird (the fuselage in our case) modifies the airflow and therefore the aerodynamics of the tail. One can see in Figure 27 that the forces generated by the tail when it is attached to the fuselage are similar until the tail stalls, when the fuselage allows for greater forces, especially lift. This implies that the

fuselage enables the airflow to hold on to the tail at higher angles of attack, increasing the stalling angle.

Finally, for a more accurate study of the aerodynamics of the avian tail, a fuselage (and preferably wings as well) needs to be attached, which was not done fully in these experiments. Moreover, in this study there was only enough time to properly test tails following one design constraint: same Reynolds number. Different hypotheses such as same aspect ratio or same area should also be tested to completely characterise the avian tail.

Chapter 9. BIBLIOGRAPHY

[1] Taylor, G. K. & Thomas, A. L. R. Animal flight dynamics II. Longitudinal stability in flapping flight. *Journal of Theoretical Biology* 351-370 (2002).

[2] Maybury, W. J. & Rayner, J. The avian tail reduces body parasite drag by controlling flow separation and vortex shedding. *The Royal Society* 1405-1410 (2001).

[3] Ajanic, E., Feroskhan, M., Mintchev, S., Noca, F. & Floreano, D. Bio-Inspired Synergistic Wing and Tail Morphing Extends Flight Capabilities of Drones. *Science Robotics* (2020).

[4] Thomas, A. L. R. On the aerodynamics of birds' tails. *Philosophical Transactions: Biological Sciences* **340**, 361-380 (1993).

[5] Ömer Faruk Buyukluoglu, H. B. Aerodynamic performance analysis of airfoils by using cfd method (2015).

[6] John D. Anderson, J. Fundamentals of aeordynamics (*McGraw-Hill, Inc*., 1991).

[7] Thomas, A. L. R. Why do birds have tails? The tail as a drag reducing flap, and trim control. *Journal of theoretical biology* 247-253 (1996).

[8] Payzuk. (n.d.). *Una paloma blanca voladora libre aislada en un fondo negro. Pájaro de paz. Correo de paloma.* [Photograph]. Shutterstock. Retrieved May 25, 2021 from https://www.shutterstock.com/es/image-photo/free-flying-white-dove-isolated-on-529097335 (

[9] [Btpi-1.jpg]. (n.d.). The Ethogram. Retrieved May 26, 2021 from https://theethogram.files.wordpress.com/2015/02/btpi-1.jpg

[10] Speight, H. (n.d.). *Kite soaring* [Photograph]. Yorkshire Red Kites. Retrieved May 26, 2021 from http://www.yorkshireredkites.net/general/is-it-a-red-kite-or-is-it-a-buzzard

[11] Sibley, D. A. (n.d.). *Swallow-tailed kite* [Photograph]. Audubon. Retrieved May 26, 2021 from https://www.audubon.org/field-guide/bird/swallow-tailed-kite

[12] Lentink, D., & de Kat, R. (2014). Gliding Swifts Attain Laminar Flow over Rough Wings. *PLoS ONE*, *9*(6), e99901. https://doi.org/10.1371/journal.pone.0099901

[13] Wikipedia contributors. (2021, April 20). *Chord (aeronautics)*. Wikipedia. Retrieved June 2, 2021 from https://en.wikipedia.org/wiki/Chord_(aeronautics)#Mean_aerodynamic_chord

[14] Ananda, G., Sukumar, P., & Selig, M. (2015). Measured aerodynamic characteristics of wings at low Reynolds numbers. *Aerospace Science and Technology*, *42*, 392–406. https://doi.org/10.1016/j.ast.2014.11.016

[15] NACA 4 digit airfoil generator (NACA 0025 AIRFOIL). (n.d.). Airfoil Tools. Retrieved June 7, 2021, from - http://airfoiltools.com/airfoil/naca4digit?MNaca4DigitForm%5Bcamber%5D=0&MNaca4DigitForm%5Bposition%5D=0&MNaca4DigitForm%5Bthick%5D=25&MNaca4DigitForm%5BnumPoints%5D=150&MNaca4DigitForm%5BcosSpace%5D=0&MNaca4DigitForm%5BcosSpace%5D=1&MNaca4DigitForm%5BcloseTe%5D=0&yt0=Plot

[16] Anwar, S. (2018, October 30). *Top 10 fastest birds in the world*. Jagranjosh.Com. Retrieved June 7 from https://www.jagranjosh.com/general-knowledge/top-10-fastest-birds-in-the-world-1540901117-1

[17] *Pigeons - everything there is to know about the pigeon - PCRC*. (n.d.). Pigeon Control Resource Centre. Retrieved June 7, 2021, from https://www.pigeoncontrolresourcecentre.org/html/about-pigeons.html

[18] *Pigeon | speed of animals*. (n.d.). Speedofanimals.Com. Retrieved June 7, 2021, from http://www.speedofanimals.com/animals/pigeon

[19] *Rock dove*. (n.d.). Animalia.Bio. Retrieved June 7, 2021, from https://animalia.bio/rock-dove

[20] ATI Industrial Automation. (n.d.). *F/T Sensor Gamma*. ATI-IA. Retrieved June 7, 2021, from https://www.ati-ia.com/products/ft/ft_models.aspx?id=Gamma

[21] ATI Industrial Automation. (n.d.-a). *ATI Industrial Automation: F/T Sensor Nano17*. ATI-IA. Retrieved June 20, 2021, from https://www.ati-ia.com/products/ft/ft_models.aspx?id=Nano17

[22] Ruffles, W. & Dakka, S. M. Aerodynamic flow characteristics of utilizing delta wing configurations in supersonic and subsonic flight regimes. *Journal of Communication and Computer* **13**, 299-318 (2016).

[23] Ahmad Z. Al-Garni, F. S. & Al-Garni, A. M. Experimental and numerical investigation of 65-deg delta and 65/40-deg double-delta wings. *Journal of Aircraft.*

[24] United Nations. (n.d.). Goal 9 | Build resilient infrastructure, promote inclusive and sustainable industrialization and foster innovation. SDGS.UN. Retrieved July 15, 2021, from https://sdgs.un.org/goals/goal9

[25] What is 3D Printing? - Technology Definition and Types. (n.d.). TWI. Retrieved July 20, 2021, from https://www.twi-global.com/technical-knowledge/faqs/what-is-3d-printing#WhatMaterialscanbeusedin3DPrinting

ANNEX I. SOURCE CODE

File tail_shapes.m, used to generate the outline of the tails.

```
%% Forked tail
clear all;
close all;

% Inputs (mm and °)
disp('Forked')
L = 291.4
e = 0.3*L
alpha = 110
edge_chord = 0.15*L;

% Geometry
alpha_rad = alpha*pi/180;
x1 = L/2;
y1 = x1/tan(0.5*alpha_rad) + edge_chord;
y2 = y1-e;

x = -x1:0.01:0; % x vector
r1 = y1 + (y1-edge_chord)/x1*x;
r2 = y2 + y2/x1*x;

%plot
figure;
plot(x, r1, x, r2, -x, r1, -x, r2, 'Color', 'blue');
grid on;
axis equal;

% Results
area = 2*(0.5*x1*(y1-edge_chord) + x1*edge_chord - 0.5*x1*y2)
AR = L^2/area

% Mean aerodynamic chord
chord_squared = @(x_var) ((y1 + (y1-edge_chord)/x1*x_var) - (y2 +
y2/x1*x_var)).^2;
MAC = 2/area * integral(chord_squared, -x1, 0)

%% Triangular tail
clear all;

% Inputs (mm and °)
disp('Triangular')
L = 250
alpha = 110
edge_chord = L/10;
```

```
% Geometry
alpha_rad = alpha*pi/180;
x1 = L/2;
y1 = x1/tan(0.5*alpha_rad) + edge_chord;

x = -x1:0.01:0; % x vector
r1 = y1 + (y1 - edge_chord)/x1*x;

%plot
figure;
plot(x, r1, -x, r1, x, 0*x, -x, 0*x, 'Color', 'blue');
grid on;
axis equal;

% Results
area = 0.5*L*(y1 - edge_chord) + L*edge_chord
AR = L^2/area

% Mean aerodynamic chord
chord_squared = @(x_var) (y1 + (y1 - edge_chord)/x1*x_var).^2;
MAC = 2/area * integral(chord_squared, -x1, 0)


%% Circulat sector tail
clear all;

% Inputs (mm and °)
disp('Circular sector')
L = 160.7
alpha = 110

% Geometry
alpha_rad = alpha*pi/180;
x1 = L/2;
y1 = x1/tan(0.5*alpha_rad);
radius = sqrt(x1^2+y1^2);

x = -x1:0.01:0; % x vector
r1 = y1 + y1/x1*x;
curve = -y1 + sqrt(radius^2 - x.^2);

%plot
figure;
plot(x, r1, x, -curve, -x, r1, -x, -curve, 'Color', 'blue');
grid on;
axis equal;

% Results
area = pi*radius^2*alpha/360
AR = L^2/area

% Mean aerodynamic chord
```

```
chord_squared = @(x_var) ((y1 + y1/x1*x_var) + (-y1 + sqrt(radius^2 -
x_var.^2))).^2;
MAC = 2/area * integral(chord_squared, -x1, 0)
```

File main.m, used to get a first glimpse of the collected data.

```
clear all;
close all force;
%% Go to folder where test data are
root_folder_name = '..\wind tests 3-5';
dir_info = dir(root_folder_name);

for folder_index = 3:length(dir_info)
    % choose subfolder
    sub_folder_name = strcat(dir_info(folder_index).folder, '\',
dir_info(folder_index).name);
    subfolder_info = dir(sub_folder_name);

    for subfolder_index = 3:length(subfolder_info)
        %% Choose dataset
        assembly = dir_info(folder_index).name;
        speed = str2num(strrep(subfolder_info(subfolder_index).name, 'm-s.csv',
''));

        %% load data
        title = assembly + " at " + string(speed) + ' m/s';
        data_nonfiltered = readmatrix(strcat(sub_folder_name, '\', string(speed),
'm-s.csv'));
        %FrequencyPlot(data_nonfiltered(:,4), title);

        %% Filter data
        sampling_frequency = GetSamplingFrequency(data_nonfiltered);
        data_filtered = lowpass(data_nonfiltered, 0.5, sampling_frequency);
        if strcmp(assembly, 'fuselage + forked') && speed == 0    % 'fuselage +
____', 'just ____', 'just fuselage'
            PlotTest(data_filtered, strcat(title, ', filtered'));
            %PlotTest(data_nonfiltered, title);
        end
        %FrequencyPlot(data_filtered(:,4), strcat(title, ', filtered'));

        %% Export data
        ExportData(data_nonfiltered, sampling_frequency, title);
    end
end
```

Function PlotTest.m, used to plot the raw data

```
function PlotTest(data, name)
%Plots all components of the test

n_samples = size(data, 1);

for i=1:6
    figure;
    plot(1:n_samples, data(:,i));
    grid on;
    xlabel('sample N°');

    if i == 1
        ylabel('Fx [N]');
        title('Fx in ' + name);
    elseif i == 2
        ylabel('Fy [N]');
        title('Fy in ' + name);
    elseif i == 3
        ylabel('Fz [N]');
        title('Fz in ' + name);
    elseif i == 4
        ylabel('Tx [Nm]');
        title('Tx in ' + name);
    elseif i == 5
        ylabel('Ty [Nm]');
        title('Ty in ' + name);
    elseif i == 6
        ylabel('Tz [Nm]');
        title('Tz in ' + name);
    end
end

end
```

File ExportDataArrays.m, used to convert the raw data collected by the load cell to the usable data that will be analysed.

```
% Exports, for every angle, wind speed and configuration, a vector with the
% samples that are going to be taken into account, projected onto a ground
reference
% This can be later used to compute the mean and the standard deviation
clear all;
close all;

%% Go to folder where test data are
root_folder_name = '..\wind tests 3-5';
export_folder_name = 'Exported data 3-5/Exported arrays/';
dir_info = dir(root_folder_name);

angle_array = [0 5 10 15 20 25 30 35 40 45]'; % degrees

for folder_index = 3:length(dir_info)
    assembly = dir_info(folder_index).name;
    % choose subfolder
    sub_folder_name = strcat(dir_info(folder_index).folder, '\',
dir_info(folder_index).name);
    subfolder_info = dir(sub_folder_name);

    for subfolder_index = 3:length(subfolder_info)
        % Choose dataset
        speed = str2num(strrep(subfolder_info(subfolder_index).name, 'm-s.csv',
''));

        % load data
        data_nonfiltered = readmatrix(strcat(sub_folder_name, '\', string(speed),
'm-s.csv'));
        sampling_frequency = GetSamplingFrequency(data_nonfiltered);

        % get the robotic arm's fisrt 'spike'
        first_spike = max(data_nonfiltered(1:1000, 3));
        first_spike_index = find(data_nonfiltered(1:1000, 3) == first_spike, 1,
'first');

        % Get array of values
        for i=1:length(angle_array) % for every angle
            value_matrix = [];
            for k=1:6 % for every force and torque
                % take some values for each angle to average them out
                start_index = first_spike_index + floor((22 + 10*(i-
1))*sampling_frequency);
                end_index = start_index + floor(2*sampling_frequency);
                value_matrix(:, k) = data_nonfiltered(start_index:end_index, k);
            end
            %value_matrix(:, 3) = 0.44+value_matrix(:, 3);
```

```
            value_matrix =  [value_matrix(:, 1)*cos(angle_array(i)*pi/180) -
value_matrix(:, 3)*sin(angle_array(i)*pi/180), value_matrix(:, 2),
value_matrix(:, 1)*sin(angle_array(i)*pi/180) + value_matrix(:,
3)*cos(angle_array(i)*pi/180), value_matrix(:, 4)*cos(angle_array(i)*pi/180) -
value_matrix(:, 6)*sin(angle_array(i)*pi/180), value_matrix(:, 5),
value_matrix(:, 4)*sin(angle_array(i)*pi/180) + value_matrix(:,
6)*cos(angle_array(i)*pi/180)];

            for k = 1:6
                value_array = value_matrix(:, k);

                if k == 1 % Fx
                    force = 'Fx';
                elseif k == 2 % Fy
                    force = 'Fy';
                elseif k == 3 % Fz
                    force = 'Fz';
                elseif k == 4 % Tx
                    force = 'Tx';
                elseif k == 5 % Ty
                    force = 'Ty';
                elseif k == 6 % Tz
                    force = 'Tz';
                end

                % Export file
                assembly_name = strrep(assembly, ' + ', '_');
                assembly_name = strrep(assembly_name, ' ', '_');
                file_name = strcat(assembly_name, '-', string(speed), '-',
string(angle_array(i)), '-', force); %assembly-speed-angle-force
                save(strcat(export_folder_name, file_name), 'value_array')
            end
        end
    end
end
```

File plots_report.m, used to visualise the data in graphs.

```
% To be used for the plots in the report

clear all;
close all;
figure1 = figure;
sgtitle('Lift and drag coefficients as function of angle of attack for each tail
shape');
coefficients = true; % calculate coefficients

%% Load data
root_folder_name = 'Exported data 9-6/Exported arrays';
filename = 'just_support-ss-xx-FF.mat'; % support (for just tails) or fuselage
(for birds)
angle_array = [0 5 10 15 20 25 30 35 40 45]' - 2; % degrees

%% Get forces of wind on fuselage (or support)
% We then store the force that the wind exerts on the fuselage
filename;
lift_fuselage = []; %angle, speed
drag_fuselage = [];
a = 0;
for angle=angle_array(1):5:angle_array(end)
    a = a+1;
    for speed = 0:2:10
        %lift
        loaded_data = load(strcat(root_folder_name, '/',
strrep(strrep(strrep(filename, 'ss', string(speed)), 'FF', 'Fz'), 'xx',
string(angle+2)))).value_array;
        lift_fuselage(a, speed/2+1, :) = loaded_data;

        %drag
        loaded_data = load(strcat(root_folder_name, '/',
strrep(strrep(strrep(filename, 'ss', string(speed)), 'FF', 'Fx'), 'xx',
string(angle+2)))).value_array;
        drag_fuselage(a, speed/2+1, :) = loaded_data;
    end
end

%% Plot
marker_colour = [51/255, 137/255, 175/255;
                 191/255, 19/255, 171/255;
                 147/255, 147/255, 33/255];
line_colour = [178/255, 215/255, 232/255;
                   246/255, 160/255, 236/255;
                   233/255, 233/255, 155/255];

for i=1:3
    if i == 1
        assembly = 'just_circular-';
    elseif i ==2
        assembly = 'just_triangular-';
```

```
    elseif i== 3
        assembly = 'just_forked-';
    end

    % Constants
    rho = 1.2041;
    if contains(assembly, 'forked')
        A= 26882e-6;
    elseif contains(assembly, 'triangular')
        A= 15617e-6;
    elseif contains(assembly, 'circular')
        A= 11588e-6;
    end

    for speed = 6:2:10
        subplot(2, 3, i); % Lift
        % get data
        lift_data = []; %data to be plotted. sorted by angle
        drag_data = []; %data to be plotted. sorted by angle
        a = 0;
        for angle=angle_array(1):5:angle_array(end)
            a = a+1;
           filename = strcat(assembly, string(speed), '-', string(angle+2), '-
Fz.mat');
           data = load(strcat(root_folder_name, '/', filename)).value_array;
           lift_data(:, a) = -(data - squeeze(lift_fuselage(a, speed/2+1, :))); %
we change the sign of the lift
        end

        if coefficients
            lift_data = 2*lift_data/(A*rho*speed^2);
        end

        % delete zero columns
        lift_data = lift_data(:,any(lift_data));
        drag_data = drag_data(:,any(drag_data));

        % Plot
        hold on;
        errorbar(angle_array, mean(lift_data), std(lift_data), 'Marker', '.',
'Color', marker_colour(speed/2-2,:), 'MarkerSize', 25, 'LineWidth', 2,
'LineStyle', 'none');
        fit_lift = fit(angle_array, mean(lift_data)', 'poly5');
        plotfit = plot(fit_lift, angle_array, mean(lift_data));
        plotfit(2).Color = line_colour(speed/2-2,:);
        plotfit(2).LineWidth = 1;
        plotfit(1).Marker = 'none';
        s=findobj('type','legend');
        delete(s);

        hold off;
        xlabel('Angle of attack [°]');
        if coefficients
```

```
            ylabel('Lift coefficient [-]');
        else
            ylabel('Lift [N]');
        end
        xlim([-5 50]);
        grid on;
        %title(title_text);
    end

    for speed = 6:2:10 % Drag
        subplot(2, 3, i+3);
         % get data
        drag_data = []; %data to be plotted. sorted by angle
        a = 0;
        for angle=angle_array(1):5:angle_array(end)
            a = a+1;
           filename = strcat(assembly, string(speed), '-', string(angle+2), '-
Fx.mat');
           data = load(strcat(root_folder_name, '/', filename)).value_array;
           drag_data(:, a) = data - squeeze(drag_fuselage(a, speed/2+1, :));
        end

        if coefficients
            drag_data = 2*drag_data/(A*rho*speed^2);
        end

        % Plot
        hold on;
        errorbar(angle_array, mean(drag_data), std(drag_data), 'Marker', '.',
'Color', marker_colour(speed/2-2,:), 'MarkerSize', 25, 'LineWidth', 2,
'LineStyle', 'none');
        fit_drag = fit(angle_array, mean(drag_data)', 'poly3');
        plotfit = plot(fit_drag, angle_array, mean(drag_data));
        plotfit(2).Color = line_colour(speed/2-2,:);
        plotfit(2).LineWidth = 1;
        plotfit(1).Marker = 'none';
        s=findobj('type','legend');
        delete(s);

        xlabel('Angle of attack [°]');
        if coefficients
            ylabel('Drag coefficient [-]');
        else
            ylabel('Drag [N]');
        end
        xlim([-5 50]);
        grid on;
    end
end
legend('6 m/s', '', '', '8 m/s', '', '', '10 m/s', '', '');
subplot(2, 3, 1);
title('Circular');
ylim([-0.2 0.8])
```

```
subplot(2, 3, 2);
title('Triangular');
ylim([-0.2 0.8])
subplot(2, 3, 3);
ylim([-0.2 0.8]);
title('Forked');
subplot(2, 3, 4);
ylim([-0.1 0.7]);
subplot(2, 3, 5);
ylim([-0.1 0.7]);
subplot(2, 3, 6);
ylim([-0.1 0.7]);
```

ANNEX II. UNITED NATION'S SUSTAINABLE DEVELOPMENT GOALS

Looking at the bigger picture, the ultimate goal of this project is to improve the flying efficiency of drones, so the UN sustainable development goals that will be affected by this will be commented here.

The primary SDG pursued by this project is goal number 9: *"Build resilient infrastructure, promote inclusive and sustainable industrialization and foster innovation"*. The kind of technology that is being developed here does not yet exist, at least at an industrial level. Drones nowadays belong mainly to one of these two kinds: a quadrotor or fixed wing aircraft.

Figure 28. Different types of drones: quadrotor (left) and fixed wing aircraft (right).

It has been discussed before that both agility and speed cannot be achieved at the same time. The quadrotor allows for great manoeuvrability but little speed, whereas a conventional unmanned aircraft works the opposite way: it can achieve great speed but is not very agile and has to be constantly moving. If this project is successful, we will have a new technology that can achieve both speed and manoeuvrability in flying aircraft (or drones, of course).

United Nations claims that one of the targets of Goal number 9 is to "enhance scientific research, upgrade the technological capabilities of industrial sectors in all countries, in particular developing countries, including, by 2030, encouraging innovation and

substantially increasing the number of research and development workers per 1 million people and public and private research and development spending" [24]. This is exactly what the project is trying to pursue: to use scientific research to improve the technological capabilities of current industrial products, drones in particular.

It is hard to quantify the impact that drones with enhanced flying capabilities will have on society, as we are just experiencing the rise of mass usage of drones. As this technology enables a new range of activities to be carried out, its impact depends on the use we, as a society, make of it. It could very well be used in warcraft, as Figure 28 suggests, however it is the improvement of infrastructure that I would like to focus on. UN states that "in the 25 countries in Africa, Asia, South America, Central Asia and the Middle East where the Rural Access Index was updated using a spatial method, almost 300 million out of 520 million rural dwellers still lack good access to roads" [24]. There is therefore plenty of need for this kind of drones; they can be used to fly over the rugged terrain or dense forests that often surround communities without access to roads to deliver goods, exchange information or carry out reconnaissance missions to better understand the relief and, perhaps, find the ideal place to build that road or a tunnel.

The example previously presented illustrates one way in which society will benefit from the research carried out in this project. It is indeed just one way this could help, however the main message here is that there is certainly a need for improved flying performance of drones and that this can be achieved though research.

ANNEX III. TECHNICAL DRAWINGS

Fuselage (manufactured in two parts)

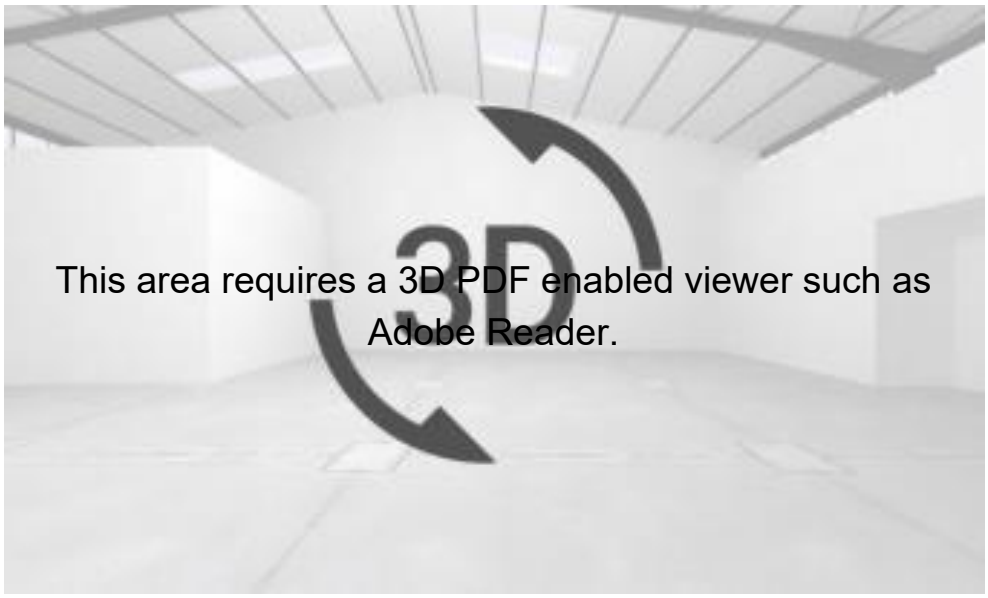

Fuselage – part 1.

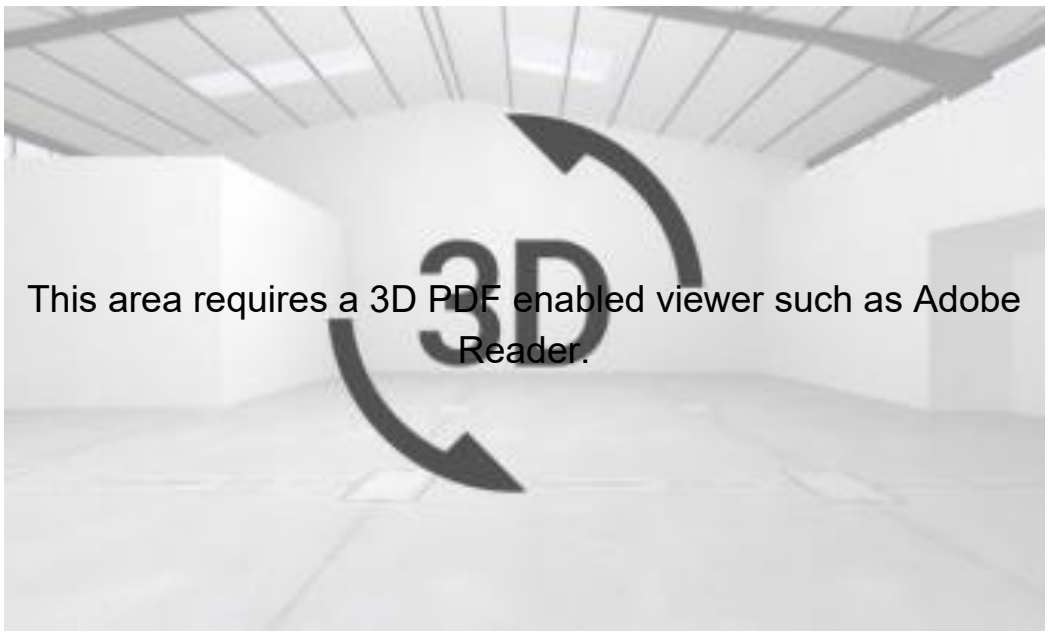

Fuselage – part 2.

Attachments

.Rod to fuselage.

Robot to load cell.

Rod to tail.

Load cell to rod

Tails (3D objects not icluded)

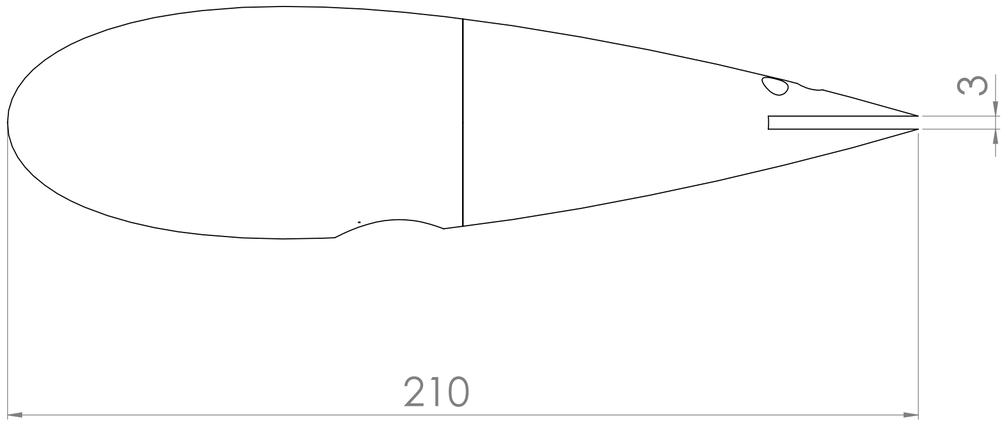

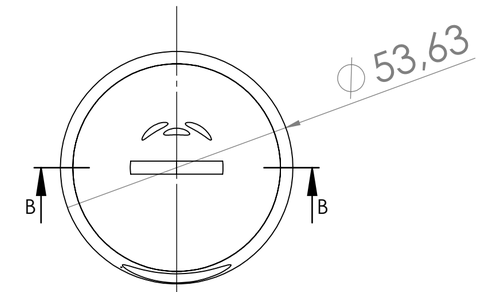

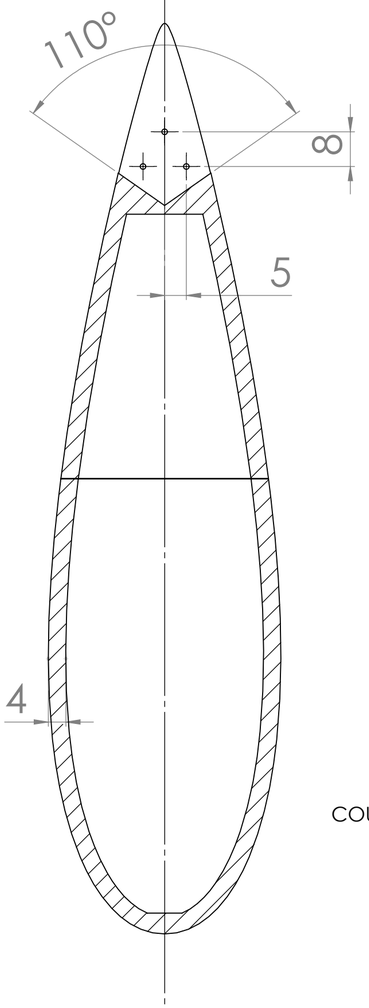

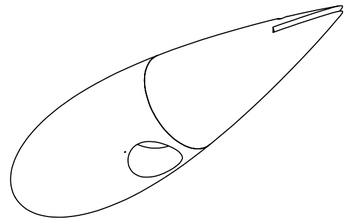

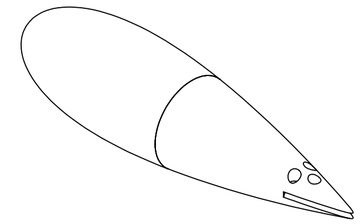

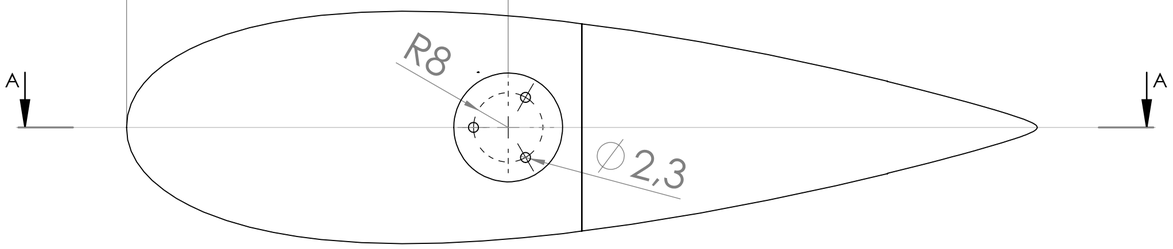

COUPE B-B

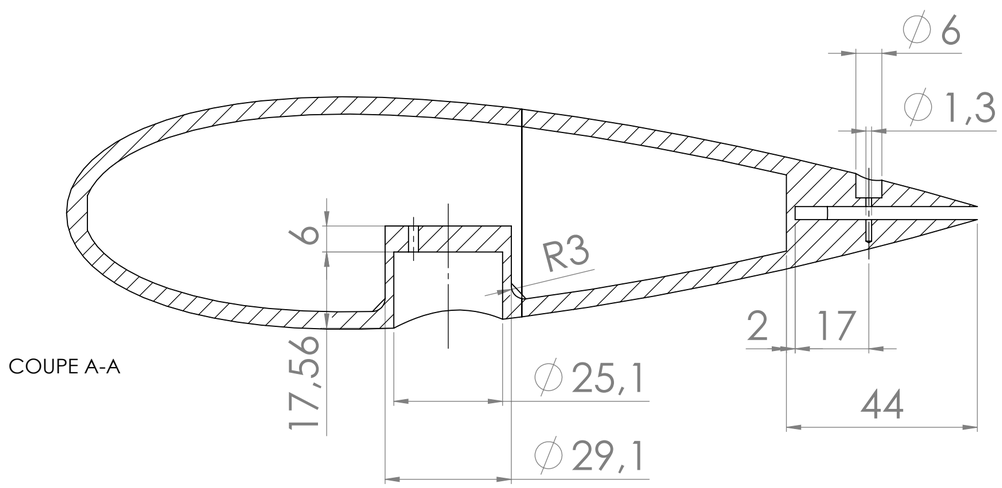

COUPE A-A

SAUF INDICATION CONTRAIRE: LES COTES SONT EN MILLIMETRES ETAT DE SURFACE: TOLERANCES: LINEAIRES: ANGULAIRES:	FINITION:		CASSER LES ANGLES VIFS	NE PAS CHANGER L'ECHELLE		REVISION	
	NOM	SIGNATURE	DATE				TITRE:
AUTEUR	A. Miguélez		03/2021				Fuselage
VERIF.							
APPR.							
FAB.							
QUAL.				MATERIAU: P 430		No. DE PLAN	A2
				MASSE:		ECHELLE:1:1	FEUILLE 1 SUR 1

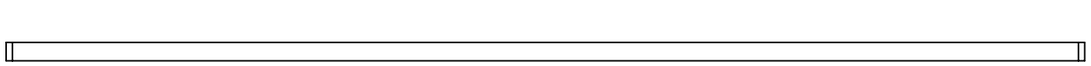

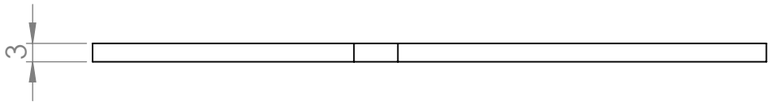

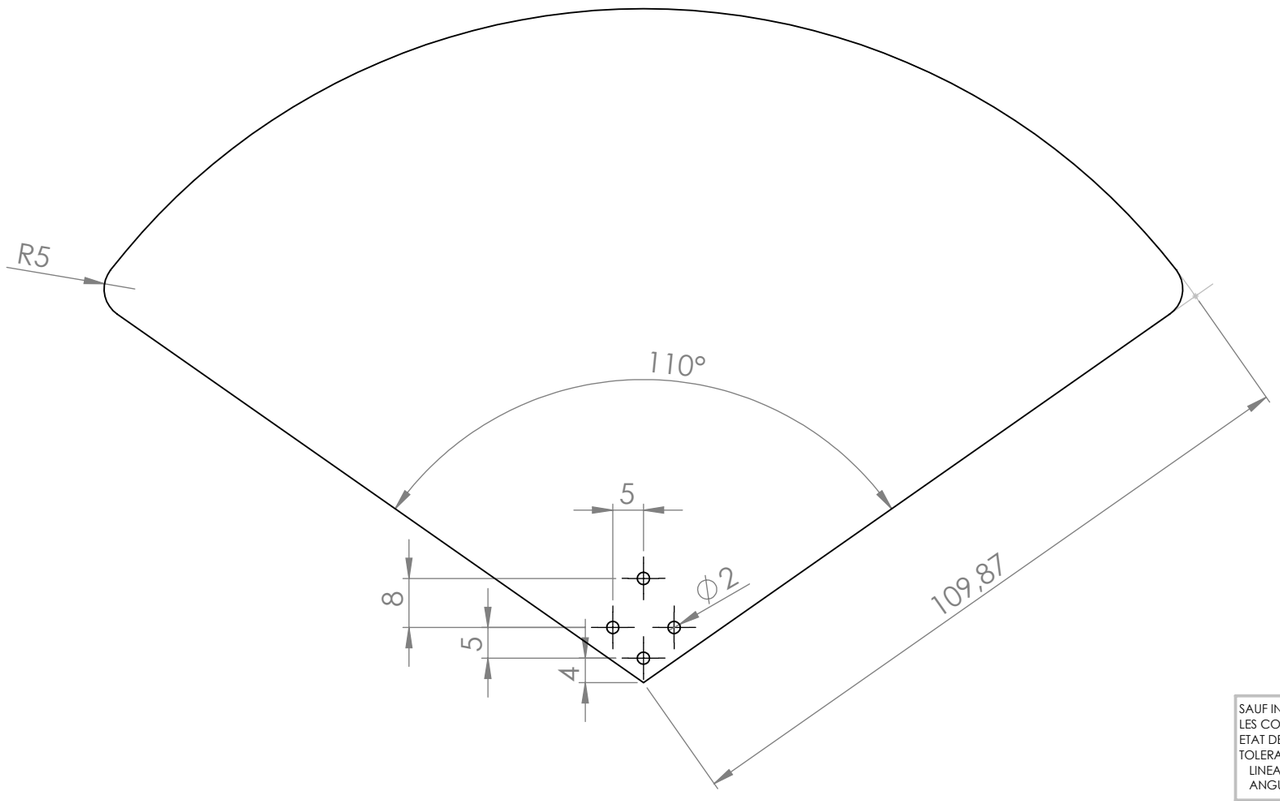

SAUF INDICATION CONTRAIRE: LES COTES SONT EN MILLIMETRES ETAT DE SURFACE: TOLERANCES: LINEAIRES: ANGULAIRES:		FINITION:		CASSER LES ANGLES VIFS		NE PAS CHANGER L'ECHELLE	REVISION
	NOM	SIGNATURE	DATE			TITRE:	
AUTEUR	A. Miguélez		03/2021			Circular tail	
VERIF.							
APPR.							
FAB.							
QUAL.				MATERIAU: FDM 3 mm		No. DE PLAN	A3
				MASSE:		ECHELLE:1:1	FEUILLE 1 SUR 1

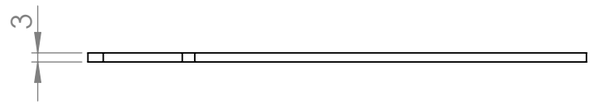

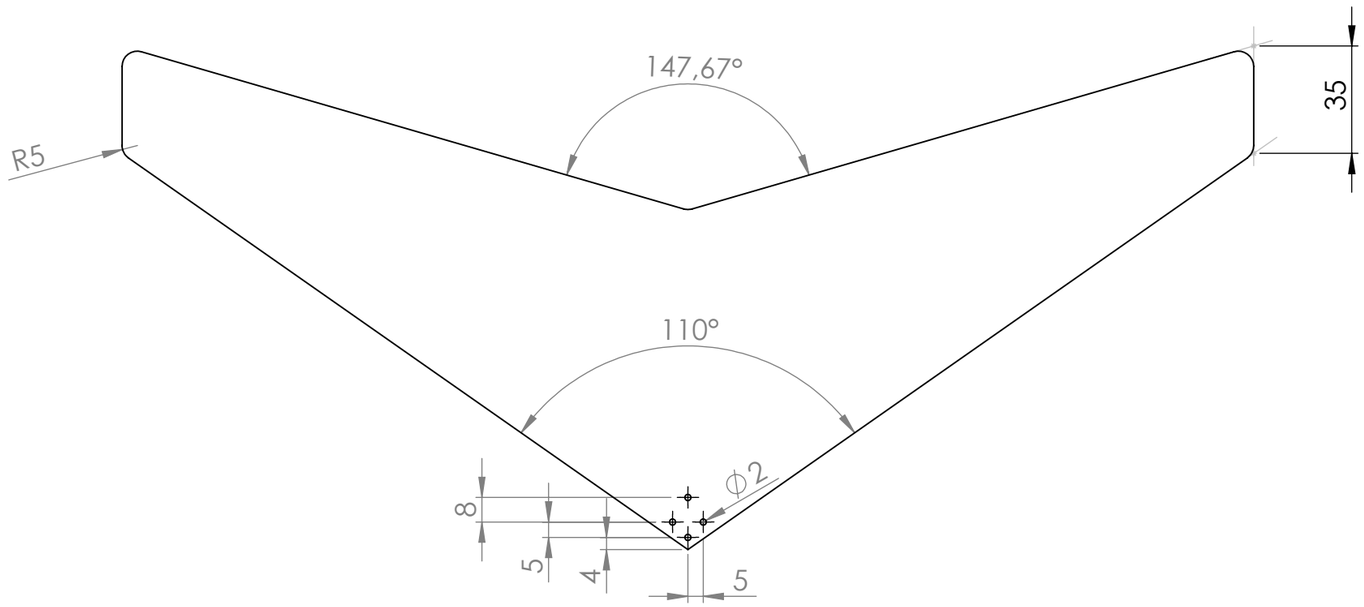

SAUF INDICATION CONTRAIRE: LES COTES SONT EN MILLIMETRES ETAT DE SURFACE: TOLERANCES: LINEAIRES: ANGULAIRES:	FINITION:		CASSER LES ANGLES VIFS	NE PAS CHANGER L'ECHELLE	REVISION		
	NOM	SIGNATURE	DATE	TITRE:			
AUTEUR	A. Miguélez		03/2021	Forked tail			
VERIF.							
APPR.							
FAB.							
QUAL.				MATERIAU: FDM 3 mm		No. DE PLAN	A3
				MASSE:		ECHELLE:1:2	FEUILLE 1 SUR 1

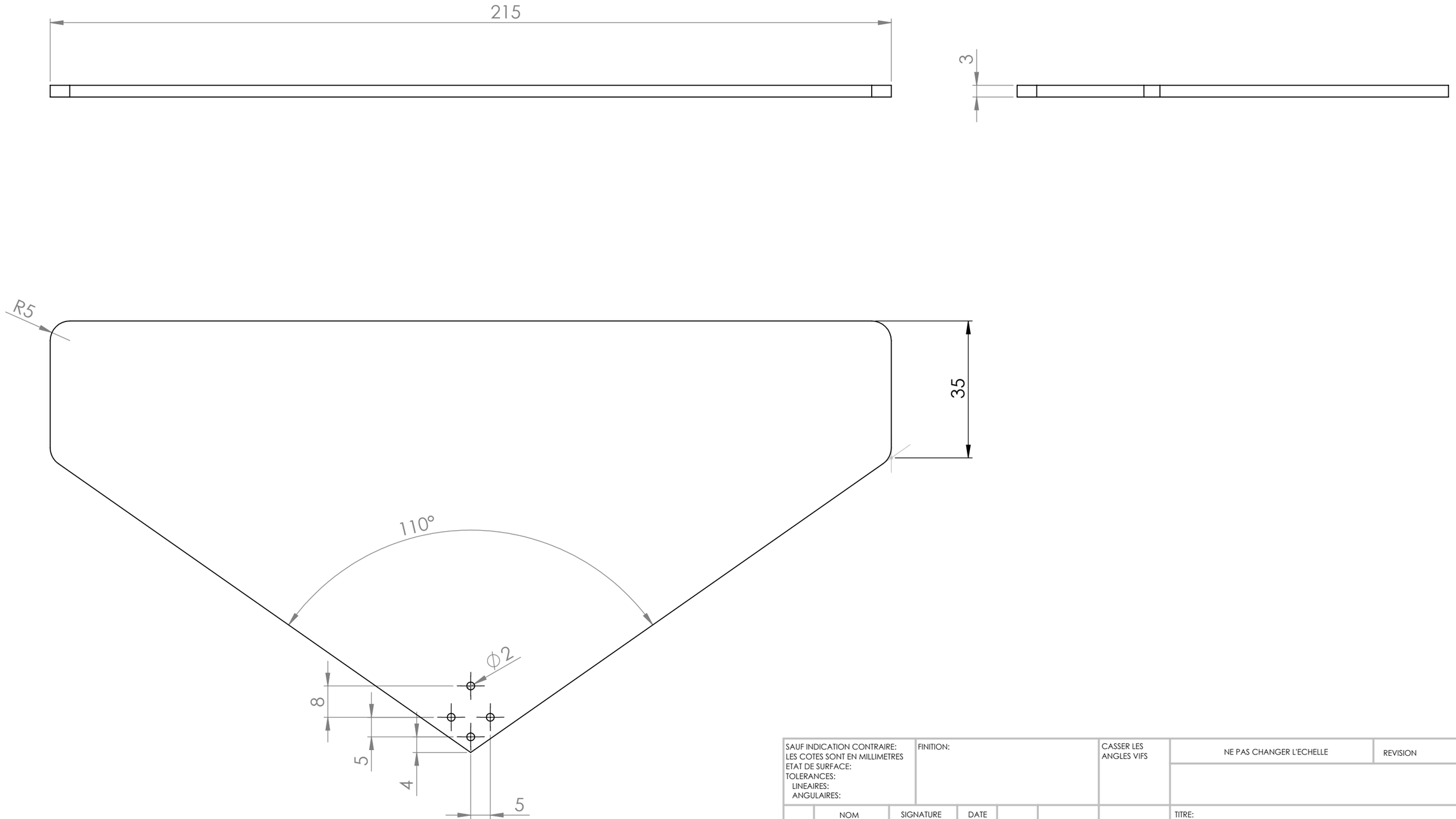

SAUF INDICATION CONTRAIRE: LES COTES SONT EN MILLIMETRES ETAT DE SURFACE: TOLERANCES: LINEAIRES: ANGULAIRES:	FINITION:		CASSER LES ANGLES VIFS	NE PAS CHANGER L'ECHELLE	REVISION		
	NOM	SIGNATURE	DATE	TITRE:			
AUTEUR	A. Miguélez		03/2021	Triangular tail			
VERIF.							
APPR.							
FAB.							
QUAL.				MATERIAU: FDM 3 mm	No. DE PLAN	A3	
				MASSE:	ECHELLE:1:1	FEUILLE 1 SUR 1	